LA-UR-99-5501
September 1999

environmental restoration project

A Department of Energy
Environmental Cleanup Program

Numerical Model of Flow and Transport for Area 2, MDA AB at TA-49

Los Alamos
NATIONAL
LABORATORY
Los Alamos, NM 87545

Produced by EES-5, Geoanalysis

Authors: Kay H Birdsell, Terry A. Cherry, Peter Lichtner and Bryan J. Travis

Table of Contents

List of Figures

List of Tables

1.0 - INTRODUCTION

Areas 2, 2A and 2B of MDA AB at TA-49 are legacy waste sites where underground nuclear safety tests were conducted in 1960 and 1961 (BMP Plan, 1998). Tests involving high explosives (HE) and special nuclear materials were conducted in six-foot diameter shafts ranging in depths from 57 to 78 feet. Plutonium, uranium-235, uranium-238, beryllium and lead were among the main constituents used in the tests. Cesisum-137 was also used as a tracer in some of the shots. The site was originally chosen because its hydrologic characteristics indicated that it would naturally contain the contaminants thus protecting groundwater. However, the hydrologic characteristics of the site were unfavorably altered in 1961 by the addition of an asphalt pad over Area 2 (OU 1144 RFI Work Plan, 1992). The pad not only inhibited evapotranspiration at this naturally dry site, it also dammed surface water along its edges and potentially channeled water through the pad into the underlying shafts. The asphalt pad was recently removed, the site has been regraded, and a surface-water diversion channel was added upstream of the site. These measures are expected to return the site's hydrologic characteristics to their naturally favorable conditions.

In this report, we present preliminary flow and transport calculations that predict the present-day, subsurface migration of uranium and cesium from Area 2. The implication for plutonium migration based on the uranium simulations is also discussed. These predictions provide estimates of radionuclide concentrations in the unsaturated zone beneath the shafts and will be used to site proposed monitoring boreholes. This process is consistent with the approach presented in the Environmental Protection Agency's (2000) Region 6, Corrective Action Strategy. As additional field data from the monitoring holes become available, the site conceptual model and the resulting numerical model and transport calculations will be updated, if needed, to support corrective actions decisions and to calculate future risk from the site.

2.0 - SITE DESCRIPTION

2.1 STRATIGRAPHY

Areas 2, 2A and 2B (PRS 49-001 (b), (c), and (d)) are located atop Frijoles Mesa at TA-49. The stratigraphy of the units located above the regional water table is shown in Figure 2-1. A soil layer that is approximately one-meter thick covers the native site (Davenport, 1996). In descending order, the next five units make up the Tshirege Member of the Bandelier tuff. The units dip gently toward the east. The Tsankawi Pumice Bed and Cerro Toledo tuffs lie between the Tshirege Member and the Otowi Member of the Bandelier Tuff (Stimac and Broxton). The Guaje Pumice and the Puye Formation lie at the base of the unsaturated zone. The water table is located at a depth of approximately 1200 feet below the ground surface.

Only a few fractures were noted in the core from hole 49-2901, a few in the first 35 feet that may influence flow near the surface, and four sub-vertical fractures with mineral coating from 243 to 255 feet, near the center of Unit 2 (Stimac and Broxton).

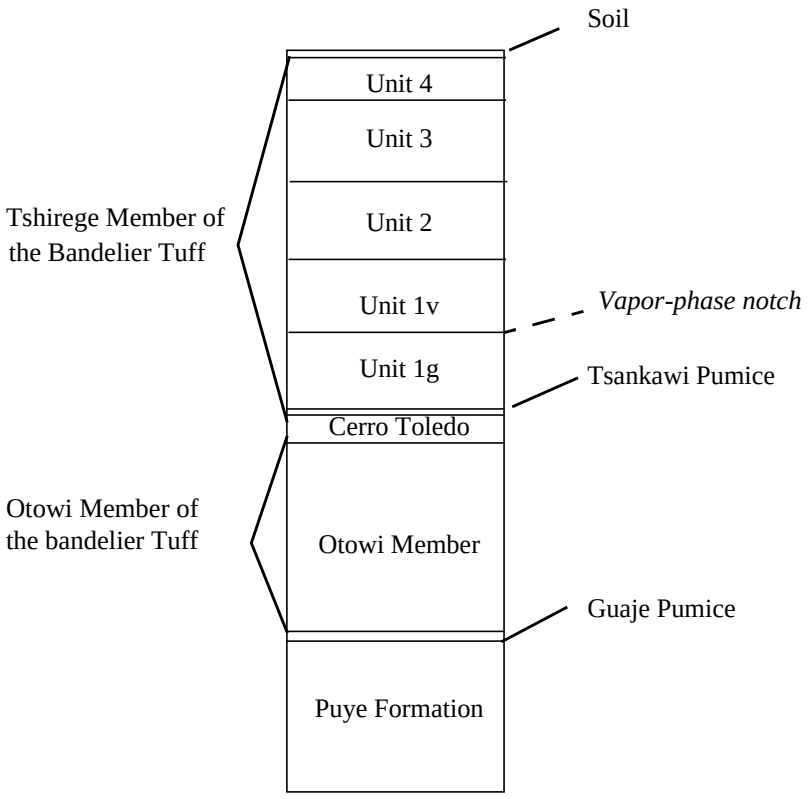

Figure 2-1. Site stratigraphy.

Area 2 (Figure 2-2) was covered with a one- to six-foot layer of compacted clay and gravel and then paved with four to six inches of asphalt in September, 1961. This elevated asphalt pad created drainage problems that led to frequent ponding in Areas 2A and a portion of Area 2B, as shown in Figure 2-2.The asphalt and some of the fill was removed in August, 1998. The surface was also regraded to promote drainage and a crushed tuff cover was added.

2.2 CONTAMINANT SOURCE

The source information in this paragraph is derived from the OU 1144 RFI Work Plan (1992). Areas 2, 2A and 2B occupy approximately 30,000 ft^2 atop Frijoles mesa at TA-49 with waste located at the bottom of six-foot diameter shafts that are 57 to 78 feet deep and spaced at 25-foot intervals, as shown in Figure 2-2. The waste was generated in 1959 and 1960 by 29 underground hydronuclear experiments involving high-explosive (HE) dispersal of special nuclear materials (SNM). The high explosives are thought to have been completely consumed by the detonation. The waste's major constituents are plutonium, uranium, lead and beryllium. Twenty of the shots were plutonium experiments that also contained U-238 and, in some cases, U-235. Three shots used U-235 and U-238, and three shots used only U-238. Also, small quantities of cesium were used as tracers in three HE experiments. The source terms for Areas 2, 2A and 2B are well known, as shown in Table 2-1. However, the quantities of radionuclides used in each experiment are classified information and therefore not presented with these scoping calculations. .

Table 2-1. Contaminant Inventory at MDA AB (from OU 1144 RFI workplan, Table 7.101, 1992). Pu is >93% Pu-239.

	Pu (kg)	U-235 (kg)	U-238 (kg)
Area 2	12.62	47.4	52.5
Area 2A	3.75	9.8	10.6
Area 2B	5.67	6.4	14.7

The nuclear materials were dispersed at the bottom of the shafts, which were filled to ground level with either sand or crushed tuff. Additional fill was added to top off the shafts following compaction, and the shafts were then covered with a concrete cap. The underground detonations caused local fracturing of the tuff units surrounding the shaft bottoms. HE containment

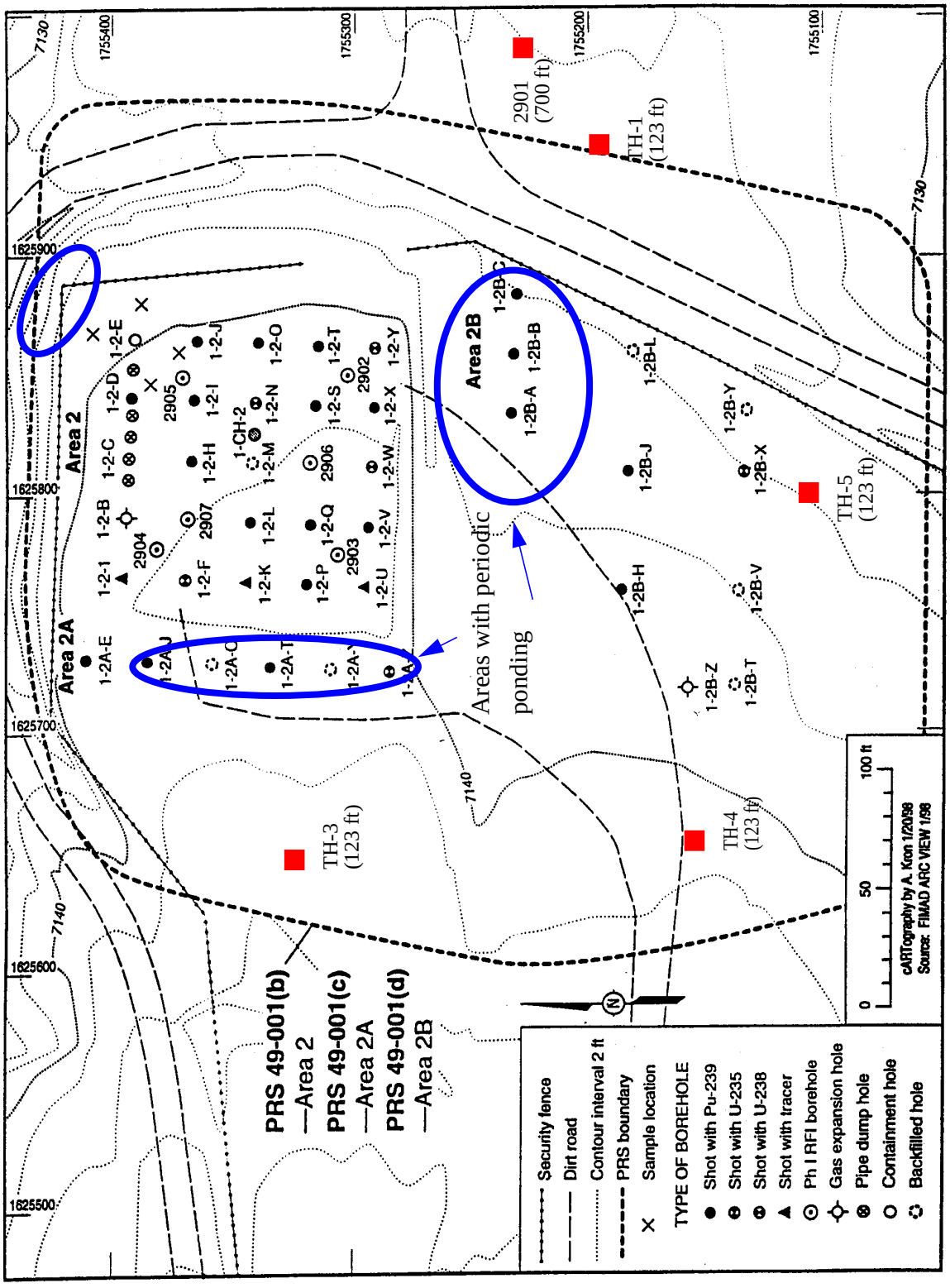

Figure 2-2. Shaft and borehole locations, and historic use (from BMP Plan (1998)).

experiments, performed prior to the hydronuclear tests, limit the radius of fracture and contaminant dispersal to 10 to 15 feet. In general, the containment experiments used larger quantities of HE than the SNM experiments (OU 1144 RFI Work Plan, 1992). The SNM (plutonium and uranium) and the cesium tracer are expected to have dispersed throughout the HE-induced fracture zone upon detonation (Kunkle, pers. Communication, 1999). Evidence from atmospheric testing of nuclear weapons shows that plutonium and uranium react to form uranium-plutonium oxide particles (UO_2 - PUO_2, UO_3) and that plutonium also interacts with soil materials to form particles. Some of these particles are of colloidal size (1 micron or less (Stumm and Morgan, 1981)), but most are larger (Shreve and Thomas, 1965), as shown in Figure 2-3. We assume that particles also form upon

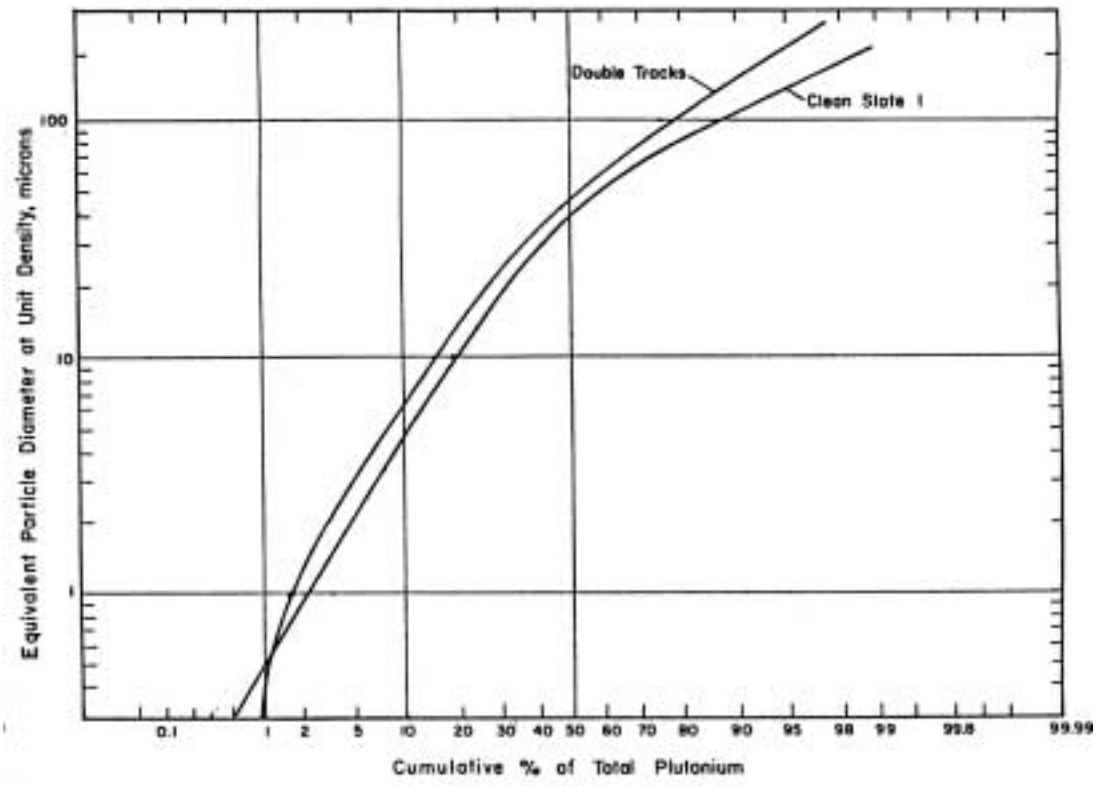

Figure 2-3. Particle size distribution for atmospheric shots, from Shreve and Thomas (1965).

detonation in the subsurface. Therefore, the initial source term for contaminant migration consists of particles uniformly distributed throughout the detonation-induced fracture zone with a particle-size distribution similar to that presented in Shreve and Thomas (1965).

2.3 HYDROLOGIC DATA

2.3.1 Moisture Content Data

Field and laboratory-derived moisture content data are useful information for predicting vadose-zone water flux and contaminant transport rates at a site. Moisture content has been measured in several boreholes surrounding Area 2 (Fig. 2-2): Borehole 49-2901 (700 ft hole) when it was drilled in 1993 and Boreholes TH-1, TH-3, TH-4 and TH-5 in February, 1996, March, 1996 and August, 1996. The moisture content in these holes, shown in Figures 2-4 and 2-5, is assumed to represent background conditions beneath the mesa top. Moisture content is generally quite low, 10% by volume or less, except in the upper 10 feet and at a depth of about 400 feet, coincident with the Unit 1v/Unit 1g contact, equivalent to the vapor-phase notch in surface exposures as shown in Figure 2-1 (Simac and Broxton, unpublished).

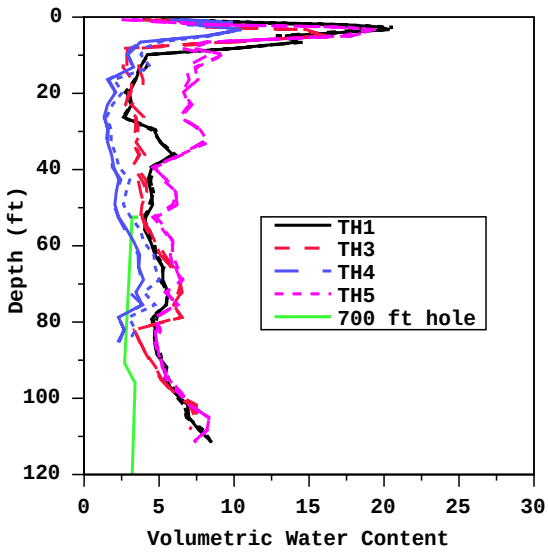

Figure 2-4. Volumetric Moisture Content data to 120 feet for wells TH1, TH3, TH4, TH5 and 49-2901 (700_foot hole). These wells surround the site and are assumed to represent background conditions.

Wetter conditions were measured beneath the asphalt pad. Gravimetric moisture content was measured in the four ten-foot-deep boreholes (49-2902, 49-2903, 49-2904, and 49-2905) and the two 150-foot-deep boreholes (49-2906 (150-1), 49-2907 (150-2)) located beneath the asphalt pad (Fig. 2-2) in February 1994. The results of these surveys are shown in Figures 2-6 and 2-7, respectively.

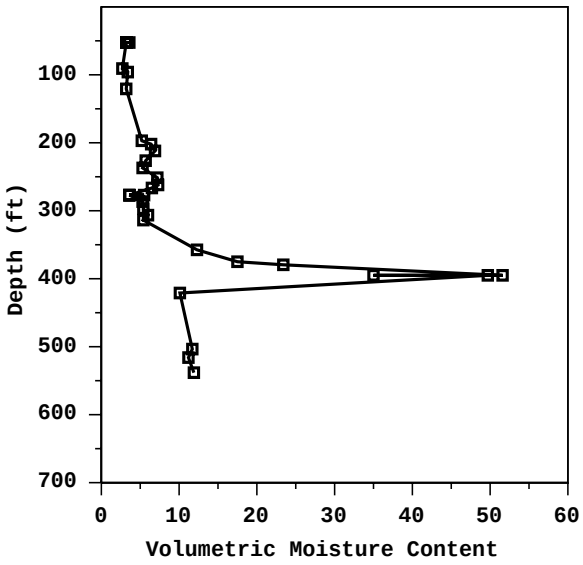

Figure 2-5. Volumetric Moisture Content data for the 700-foot deep borehole 49-2901. This well is adjacent to the site and is assumed to represent background conditions

.

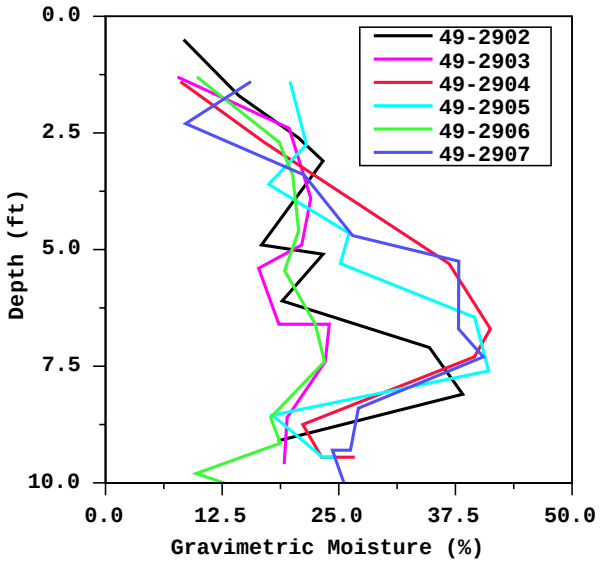

Figure 2-6. Gravimetric Moisture data to a depth of 10 feet for wells 49-2902, 49-2903, 49-2904, 49-2905, 49-2906 and 49-2907. Measured in February, 1994. These wells are located beneath the asphalt pad and represent a transient condition.

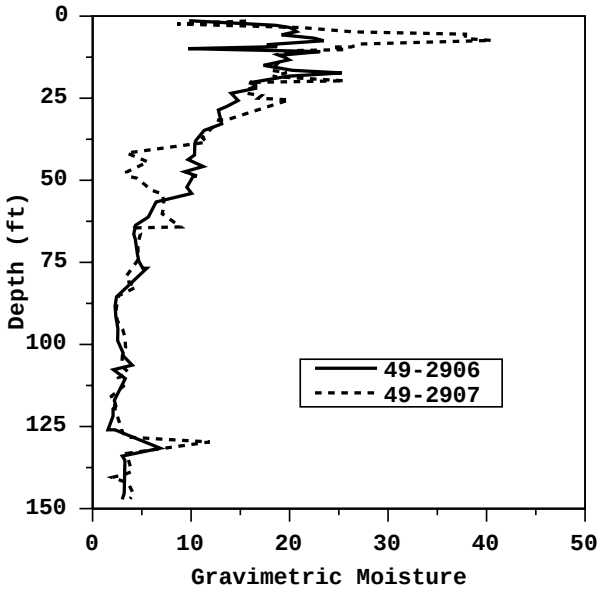

Figure 2-7. Gravimetric Moisture data to a depth of 150 feet for wells 49-2906 and 49-2907. Measured in February, 1994. These wells are located beneath the asphalt pad and the data represent transient conditions.

Volumetric moisture content was also measured in Corehole 2 (CH-2) (Figure 2-8) in late July 1998. The moisture content for this hole, which is also located beneath the asphalt pad, is much wetter than for boreholes 49-2906 and 49-2907 (Figure 2-7). The higher moisture is believed to be local to CH-2 because of its history. A large volume of water was added to the borehole and formation when it was drilled in 1959. Also, water levels monitored periodically in CH-2 between 1975 and 1998 were found to be quite variable. Water levels were 50 to 150 feet between 1975 and 1980 after the collapse over Shaft 2M. This water was eventually bailed when the water level did not drop below 150 feet for approximately two years. The hole stayed dry for seven years, then filled again to 100 feet following cracking in the asphalt. All of these moisture data are used to calibrate the numerical model so that the simulation results represent observed conditions.

Ponded areas were periodically observed over most of Area 2A and the northeastern part of Area 2B before the completion of the BMPs. However, neither the frequency and duration of their existence, or the depths of these ponds was documented. The vegetation in these areas, while the pad was in place, required more water than the plants that are native to the mesa. The only moisture data that exist for Areas 2A and 2B are from Shafts 2A-O, 2A-Y, and 2B-Y (Fig. 2-2) as shown in Figure 2-9. These data sets were collected between December, 1995 and March, 1996 and then again in August, 1998. These data do not extend into the native tuff. Shafts 2A-O and 2A-

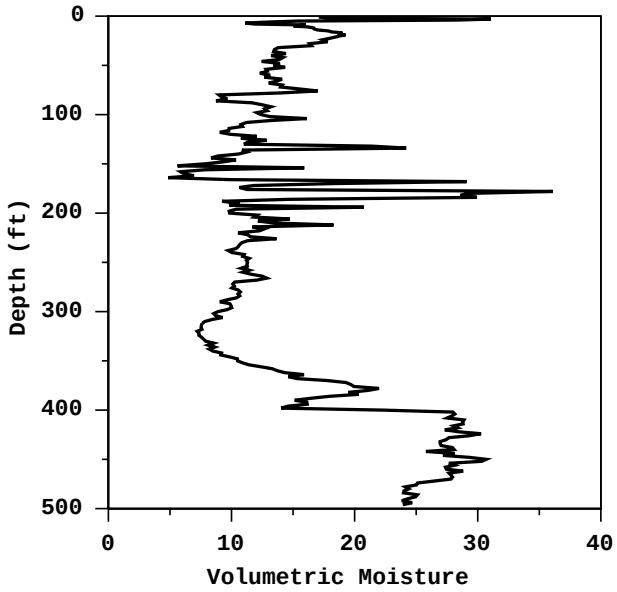

Figure 2-8. Volumetric Moisture Content data to a depth of 500 feet for Corehole 2 (CH-2). Measured in July, 1998. This well was located beneath the asphalt pad and the data represent transient conditions.

Y are located in an area where ponds were observed. Shaft 2B-Y is located about 50 feet from borehole TH-5 in an area that should have conditions similar to the site's native conditions. These data are not explicitly used in the modeling, but are included as part of a qualitative analysis of infiltration in Areas 2A and 2B.

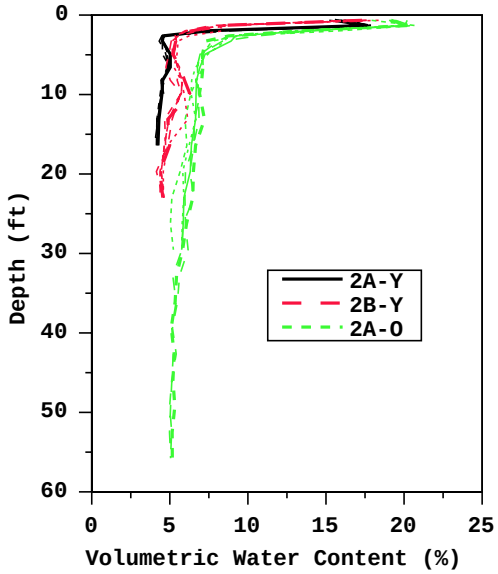

Figure 2-9. Volumetric Water Content in Shafts 2A-O, 2A-Y and 2B-Y.

2.3.2 Material Properties

This study focuses on the unsaturated zone surrounding and beneath the experimental shafts in Area 2. The van Genuchten model (van Genuchten, 1980) is used to represent the unsaturated characteristic curves for the hydrostratigraphic units, as shown in Table 2-2. The soil properties come from two soil horizons at TA-16 (Brandes, 1998). Site-specific hydrologic properties for Unit 4, Unit 3, Unit 2, Unit 1v, Unit 1g and the Otowi Member were measured on core samples from well 49-2901 (Springer, pers. Communication, 1999). Properties for the Cerro Toledo, Otowi Member and the Puye Conglomerate were the same as those used in the TA-54, MDA G performance assessment (PA) calculations (Birdsell et al., 1997). The shafts are assumed to be filled with crushed tuff backfill and again properties from the MDA G PA (Birdsell et al., 1997) are used. Estimated values for the saturated conductivity and porosity of the Puye Conglomerate (Purtymun, 1984) are used, and we assume that the van Genuchten properties are similar to those of a coarse sand.

Table 2-2. Hydrologic Properties

Mean values from [a]E. Springer, 1999, [b]Springer, 1997, [c]Purtymun (1984), [d]Carsel and Parrish (1988), [e]Brandes (1998), [f]data from 700 ft well.

Unit	Ksat (cm/s)	porosity	van Genuchten parameters $\theta s, \theta r, \alpha\ (cm^{-1}), n$
[b]Pit (Crushed Unit 2 Tuff)	2.89×10^{-4}	0.479	0.479, 0.00767, 0.00663, 2.00389,
[e]Soil (A)	2.17×10^{-5}	0.446	0.402, 0.116, 0.00855, 1.587
[e]Soil (B/CR)	1.32×10^{-7}	0.457	0.441, 0.210, 0.00577, 1.294
[a]Unit 4	9.0×10^{-5}	0.478	0.475, 0.00018, 0.00667, 1.685
[a]Unit 3	6.0×10^{-5}	0.356	0.336, 0.0, 0.0051, 1.785
[a]Unit 2	1.0×10^{-5}	0.285	0.277, 0.00092, 0.00232, 2.073
[a]Unit 1v	3.0×10^{-5}	0.473	0.395, 0.0, 0.00366, 1.652
[a]Unit 1g	7.0×10^{-5}	0.493	0.408, 0.0, 0.00715, 1.42
[?]Tsankawi Pumice	2.5×10^{-4}	0.499	0.471, 0.0049, 0.01528, 1.50
[f]Cerro Toledo	2.0×10^{-4}	0.504	0.451, 0.0214, 0.00523, 1.49
[a]Otowi Member	5.0×10^{-5}	0.493	0.441, 0.0, 0.00718, 1.604
[b]Guaje Pumice	1.5×10^{-4}	0.667	0.56, 0.0, 0.00081, 4.0264
[c,d]Puye Formation	4.6×10^{-3}	0.25	0.25, 0.045, 0.145, 2.68

The pore-size distribution is an important material property when considering the transport of colloidal particles through a porous medium. Pore sizes have not been measured on Bandelier Tuff samples. Instead, pore-size distributions measured on Yucca Mountain tuff samples are used in these calculations until site specific data can be obtained. Distributions for the Topopah Spring unit and the Calico Hills unit (Travis and Nuttall, 1987) are shown in Figure 2-10.

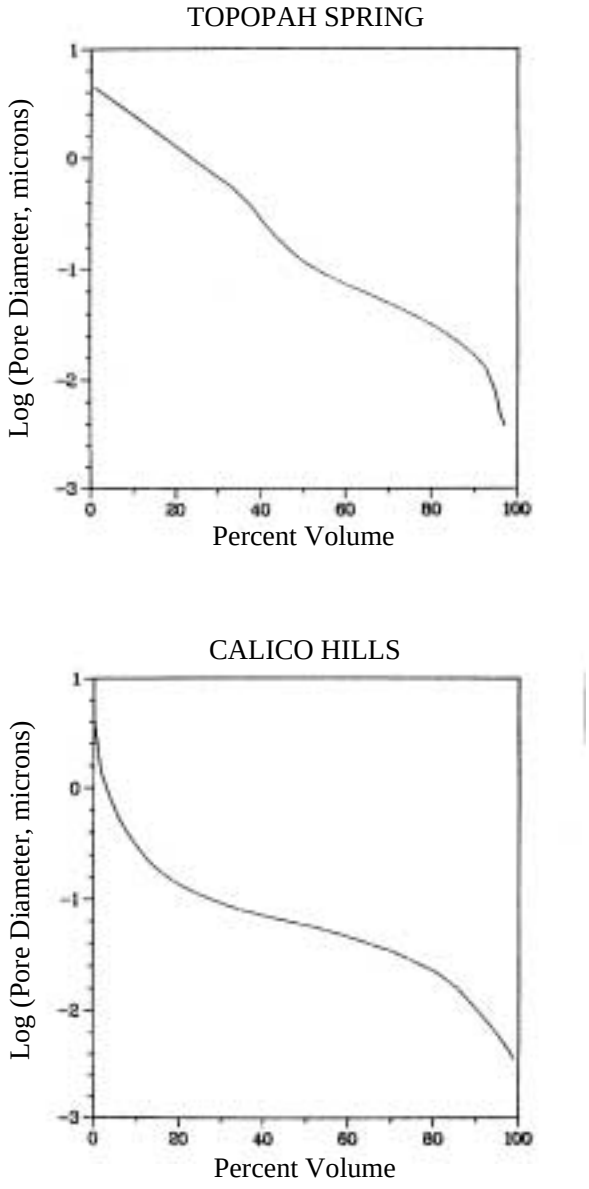

Figure 2-10. Pore-size distributions for the Topopah Spring and Calico Hills tuff at Yucca Mountain (Travis and Nuttall, 1987)

2.4 CONTAMINANT TRANSPORT DATA

2.4.1 Subsurface Contaminant Distributions

No elevated levels of radioactivity were found in samples from the two 150-foot boreholes (49-2906 and 49-2907) located beneath the asphalt pad. The same is true of samples from the 700-foot borehole (49-2901) located approximately 150 feet to the southeast of the pad. These samples were collected in order to assess the lateral migration of nuclides between boreholes and away from the site. It appears that subsurface lateral migration is minor. Future monitoring holes are proposed to measure vertical migration (BMP Plan, 1998).

So far, the only elevated radioactivity measured in subsurface samples was found in a 3.0 to 3.5 foot sample in borehole 49-2905 at the northeast corner of the asphalt pad. This sample was thought to be fill material rather than in soil (BMP Plan, 1998).

2.4.2 Transport Parameters

The partition coefficient, Kd of 2.4 ml/g, for uranium was measured on a local sample of intact unsaturated tuff (Longmire et al., 1996). The Kd value for cesium of 428 ml/g is based on sorption measurements for Yucca Mountain tuffs (Wolfsberg, 1980). Plutonium, which is also a constituent of concern, has a slightly larger distribution coefficient (Kd = 4 ml/g, (Longmire et al., 1996)) than uranium, and its migration is considered to be bounded by that of uranium and cesium. Site-specific values for diffusion coefficients and dispersivity are not available. We therefore estimate values of these parameters. For the unsaturated zone, the diffusion coefficient used is 10^{-10} m^2/s based on a study of Yucca Mountain tuffs (Rundberg et al., 1987). The dispersivity used is 1 m in the vertical direction and 0.1 m in the horizontal plane. The simulations should not be particularly sensitive to these parameters.

Some of the uranium is assumed to transport as colloidal particles with size distributions similar to those shown in Figure 2-3. The rest is assumed to be solubility limited based on the speciation calculation presented below.

Uranium solubility for Bandelier Tuff pore water was determined for a pore-water sample obtained from well 54-1107 at a depth of 51 feet for use in the source term for uranium transport. The analysis was based on data taken from Longmire et al. (1996). The results of a speciation

calculation are listed in Table 2-3 . A temperature of 25^{o} C was used in the calculation and the redox potential was fixed by equilibrium with the atmosphere (0.2 bars partial pressure O_2). The concentration of uranium was fixed by equilibrium with the mineral soddyite [$(UO_2)_2SiO_4.2H_2O$]. This is not unreasonable considering that the Bandelier Tuff pore water has a relatively high silica concentration, close to equilibrium with respect to amorphous silica. An extended Debye-Huckel activity coefficient algorithm was used in the calculations. The database used to obtain thermodynamic equilibrium constants is the most recent EQ3/6 database data0.com.V8.R6.

The uranium solubility can be expected to be sensitive to the pH, carbonate, calcium, and silica concentrations among others. According to the results of the speciation calculation, the predominant uranium species is U(VI) with the carbonate complex $UO_2(CO_3)_3^{-4}$ with a concentration of 2.56243 x 10^{-7} moles/L. The second most predominant species is the carbonate species $UO_2(CO_3)_2^{-2}$ with a concentration of 1.38838 x 10^{-8} moles/L. These two species make up most of the total uranium concentration thus giving the solubility limit of 2.7605 x 10^{-7} moles/L. The calculated uranium speciation is found to be supersaturated with respect to Haiweeite; however, Haiweeite is not often found in natural systems and should not be considered as the solubility-limiting phase for uranium.

Noteworthy is the high concentration of iron and aluminum resulting in supersaturation of a number of iron oxide and aluminum oxide and aluminosilicate minerals. Such high concentrations could be indicative of the presence of colloids contaminating the measured values. The presence of colloids could be an important factor to consider in the transport of uranium. Also noteworthy is the calculated supersaturation of calcite suggesting errors in the measured pH and/ or carbonate/bicarbonate. An inconsistency appears to exist in the data between the pH and reported bicarbonate and carbonate concentrations which could be the cause of the calcite supersaturation. In any case these discrepancies are not expected to greatly affect the calculated uranium concentration.

Table 2-3. Speciation of Uranium in Bandelier Tuff pore water at 25°C based on data from well 54-1007, 51 foot depth.

ionic strength = 2.8725E-02, pH = 9.1100, pe = 11.491, eh = 6.7977E-01
charge balance = 2.5917e-03

species	molality	total	act. coef.	constraint
al+++	6.5767E-19	8.5244E-06	3.0315E-01	1 total
b(oh)3(aq)	6.5116E-05	1.2178E-04	1.0000E+00	1 total
br-	5.3536E-05	5.3564E-05	8.4512E-01	1 total
ca++	1.5886E-03	1.9462E-03	5.5126E-01	1 total
cl-	8.6280E-03	8.6312E-03	8.4512E-01	1 total
f-	1.0527E-03	1.0527E-03	8.4849E-01	1 total
fe++	1.0925E-20	5.3718E-07	5.5126E-01	1 total
hco3-	1.1669E-03	1.4243E-03	8.5173E-01	7 conc
k+	4.5782E-03	4.5782E-03	8.4512E-01	1 total
mg++	4.8673E-04	6.6242E-04	5.7727E-01	1 total
na+	1.5007E-02	1.5007E-02	8.5173E-01	1 total
no3-	1.5596E-03	1.5596E-03	8.4512E-01	1 total
h+	8.8419E-10	-5.8461E-04	8.7792E-01	8 pH
sio2(aq)	1.3751E-03	1.6127E-03	1.0000E+00	1 total
so4--	4.0764E-03	4.4658E-03	5.2200E-01	1 total
uo2++	4.8178E-17	2.7605E-07	5.2965E-01	3 soddyite
o2(aq)	2.5221E-04	2.5235E-04	1.0000E+00	4 o2(g)

complex	molality	act. coef.	log K
hsio3-	2.37593E-04	0.85173	-9.9422
caso4(aq)	2.34803E-04	1.0000	2.1004
mgso4(aq)	1.54562E-04	1.0000	2.4125
co3--	1.14412E-04	0.52965	-10.325
caco3(aq)	1.09881E-04	1.0000	-7.0088
bo2-	5.66636E-05	0.85173	-9.2401
mgco3(aq)	1.58413E-05	1.0000	-7.3562
oh-	1.54970E-05	0.84849	-13.991
cahco3+	1.12785E-05	0.85173	1.0429
alo2-	8.52434E-06	0.85173	-22.879
mghco3+	3.53654E-06	0.85173	1.0329
mgcl+	1.74801E-06	0.85173	-0.13865
co2(aq)	1.69342E-06	1.0000	6.3414
cacl+	1.49446E-06	0.85173	-0.70039
fe(oh)3(aq)	3.88734E-07	1.0000	-3.5106
uo2(co3)3----	2.56243E-07	7.36475E-02	-9.4530

complex	molality	act. coef.	log K
caoh+	1.87091E-07	0.85173	-12.850
fe(oh)4-	1.47690E-07	0.85173	-13.111
h2sio4--	4.79357E-08	0.52200	-22.960
nabr(aq)	2.51121E-08	1.0000	-1.3623
uo2(co3)2--	1.38838E-08	0.52200	-3.7613
cacl2(aq)	1.03406E-08	1.0000	-0.65346
uo2(oh)3-	3.84355E-09	0.85173	-19.222
kbr(aq)	3.16844E-09	1.0000	-1.7423
uo2(oh)2(aq)	2.05227E-09	1.0000	-10.315
fe(oh)2+	7.57446E-10	0.85173	2.8194
(uo2)2co3(oh)3-	1.25255E-11	0.85173	-11.223
uo2(oh)4--	1.25910E-13	0.52200	-33.029
(uo2)3(oh)7-	1.02188E-17	0.85173	-31.051

Mineral Saturation Indices

mineral	SI	log	K	mineral	SI
uraninite	-25.69	-29.112	uranophane	-4.592	-17.285
uo2(am)	-30.63	-34.057	quartz	1.144	4.0056
uo2co3	-6.359	4.1266	chalcedony	0.8728	3.7344
u(co3)2	-62.27	-41.470	sio2(am)	-0.1417	2.7200
uo3(alpha)	-7.012	-8.6385	gibbsite	0.8738	-7.7559
uo3(beta)	-6.683	-8.3103	k-feldspar	7.036	0.29422
uo3(gamma)	-6.080	-7.7067	albite	4.515	-2.7458
uo2(oh)2(bet	-3.320	-4.9465	muscovite	10.43	-13.567
boltwoodite	-9.423	-14.886	analcime	3.248	-6.1267
haiweeite	8.287	7.0413	goethite	5.055	7.9553
rutherfordin	-6.383	4.1025	hematite	11.07	16.870
schoepite	-3.208	-4.8344	magnetite	-1.294	6.5057
sklodowskite	-1.593	-13.791	calcite	1.195	-1.8542
soddyite	0.	-0.39200	magnesite	0.2575	-2.2985
coffinite	-25.33	-25.893	sepiolite	11.10	-30.407
colemanite	-16.31	-21.515			

gas	log partial pressure	pressure	log K
o2(g)	-0.6990	0.2000	2.8993
co2(g)	-4.304	4.9716E-05	7.8092

3.0 - CONCEPTUAL MODEL

The OU 1144 RFI Work Plan (1992) stated that transport of contaminants through the unsaturated zone to the aquifer is not a pathway of immediate concern because of the very thick unsaturated zone and the low percolation rate at the site. The movement of contaminants by percolating water in the unsaturated zone is expected to occur primarily as suspended solids. Although fractures may facilitate contaminant transport, this should only occur above a critical water content. Therefore, matrix flow is expected to be the dominant transport mechanism and a porous medium continuum model should apply. Significant saturated flow is unlikely, but transient, rather than steady conditions, may describe near surface conditions.

The Best Management Practices (BMP) Plan (1998) supplemented the original conceptual model by summarizing the asphalt pad's effects on local moisture accumulation. "In brief, there are four aspects to the moisture accumulations of Areas 2, 2A and 2B. The foremost is the presence of the asphalt pad which traps moisture in the subsurface; secondly, the asphalt pad concentrates runoff into cracks and areas adjacent to the pads; third, poor drainage around the asphalt pad results in ponding and enhanced infiltration of water; and lastly, surface and subsurface runon from upgradient areas can contribute additional water to the immediate vicinity of Areas 2, 2A, and 2B." The plan also suggested that interflow along the soil/tuff interface may occur periodically at the site causing laterally flowing water to divert down the sand-filled shafts.

The activities proposed in of the BMP Plan were successfully implemented during 1998. These components included the construction of an upgradient trench to divert surface and subsurface runon, the removal of the asphalt pad, surface regrading to improve drainage and the addition of a crushed tuff cover. These improvements should decrease infiltration at the site to near background conditions. Therefore, the site conceptual model includes a period of enhanced infiltration from 1961 to 1998 caused by the presence of the asphalt pad followed by a return to near background conditions. Future moisture monitoring at the site will be used to confirm whether infiltration has indeed decreased.

The release of uranium is expected to be solubility limited. However, we also consider a small fraction of the uranium to be transported as extremely small particles - colloids on the order of the smallest pore sizes (i.e., the wet portion of the pore-size distribution). Cesium is expected to be infinitely soluble with its entire inventory immediately available for transport. Once released

from the source region, the mobility of the nuclides through the unsaturated zone is expected to be most strongly controlled by the water percolation rate and by the nuclide's Kd value, although matrix diffusion and dispersion are also included. Colloidal particles are not expected to adsorb onto the matrix material or to diffuse into the matrix. However, the pores of the matrix will filter the larger particles.

4.0 - NUMERICAL MODEL

4.1 OVERVIEW

The unsaturated-zone model is a two-dimensional (x,y) representation of the hydrogeologic system (Figure 4-1). The model incorporates a single six-foot diameter shaft of depth 65 feet that ends in Unit 4. (A deeper 78-foot shaft ending in Unit 3 may be considered in future modeling.) The transport pathway considered is downward migration through the unsaturated zone. Predictions of the current location of the contaminants are made in order to site monitoring holes. Predictions are also made to assess the effectiveness of the 1998 BMPs. For this, we predict 100 years into the future to compare the transport that would result if no site changes had been made to the transport that we expect will result with the completion of the BMPs.

The simulations are run with FEHM, a two- or three-dimensional finite-element code suitable for simulating systems with complex geometries that arise when modeling subsurface flow and transport (Zyvoloski et al., 1997). In the unsaturated zone, the governing equations for flow arise from the principles of conservation of water and air. Darcy's law is assumed to be valid for the momentum of the air and water phases in the unsaturated zone and for the water phase in the saturated zone. The convection-dispersion equation governs solute transport (Zyvoloski et al., 1997; Jury et al., 1991) in these analyses.

4.2 COMPUTATIONAL GRID

Defining the geometry of the geologic framework is the first step in grid generation, and can be input in terms of bounding surfaces. The geologic framework for the unsaturated-zone model was derived from the LANL site-wide geologic model (Vaniman et al., 1996) in the form of surface files. These files contain a list of elevations for all units from the surface to the water table, from State Plane coordinates (1625500, 1755100) to (1626000, 1755500) at 50’ spacing. These surfaces were refined to 25-foot spacing during grid generation, and a soil layer was added to about 5 feet below the top surface. Computational nodes were then distributed within the volume of the geometry by filling the regions between the provided surfaces with pyramid shapes, which are then converted to tetrahedral elements. Refinement in the vertical direction was done during

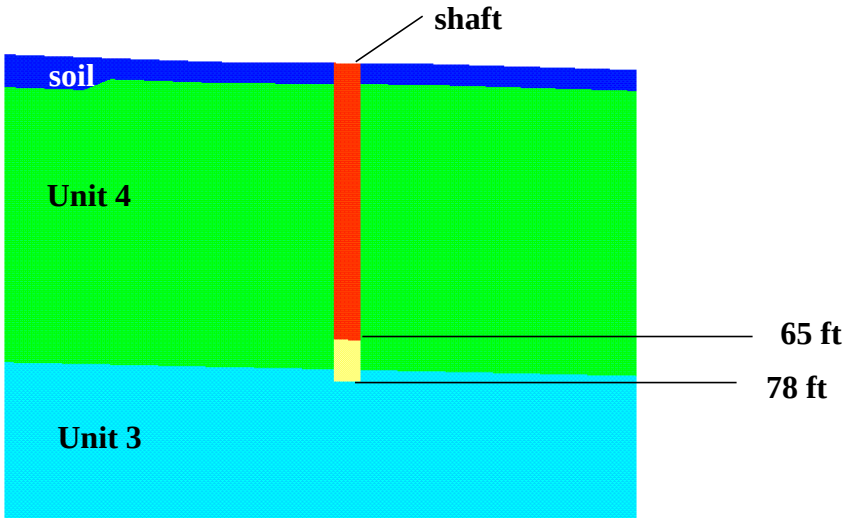

Figure 4-1. Diagram showing shaft placement in numerical model. Both shafts have a width of 6 feet. The shorter shaft shown in red is 65 feet deep. The long shaft is 78 feet deep and is shown as the combined red and yellow materials.

this process. Vertical refinement (about 6 foot spacing) is performed on several units, in particular Unit2, Unit3, and Unit4. The bottom of the mesh is truncated by the water table. This process and the resulting grid are shown in Figure 4-2. When complete, the resulting three-dimensional grid was checked for geologic accuracy and for possible grid errors, and was found to satisfy all criteria for good mesh quality.

For these preliminary FEHM calculations, a two-dimensional slice was extracted from the three-dimensional grid at y =1755350 feet (535030.68 meters) and for x = 1625500 to x = 1626000 feet, as shown in Figure 4-3. The resulting slice is made up of triangular elements.The two-dimensional grid was then further refined to include a shaft (see Figure 4-1) by adding nodes at and around the location of a typical shaft. Two grids with different shaft depths were generated, one of 65 feet and a second of 78 feet. Both shafts are 6 feet wide. Additional points are added around the shaft so that the change from fine to coarse refinement is gradual. Once refinement was complete and the points in place, points within the shaft location were selected and colored differently than the rest of the grid. This allowed the shaft points to be treated as a material separate from the geologic units. This process yielded a grid with regularly spaced elements all vertically aligned, which may allow grid orientation effects towards the vertical. This is not a problem if this is the

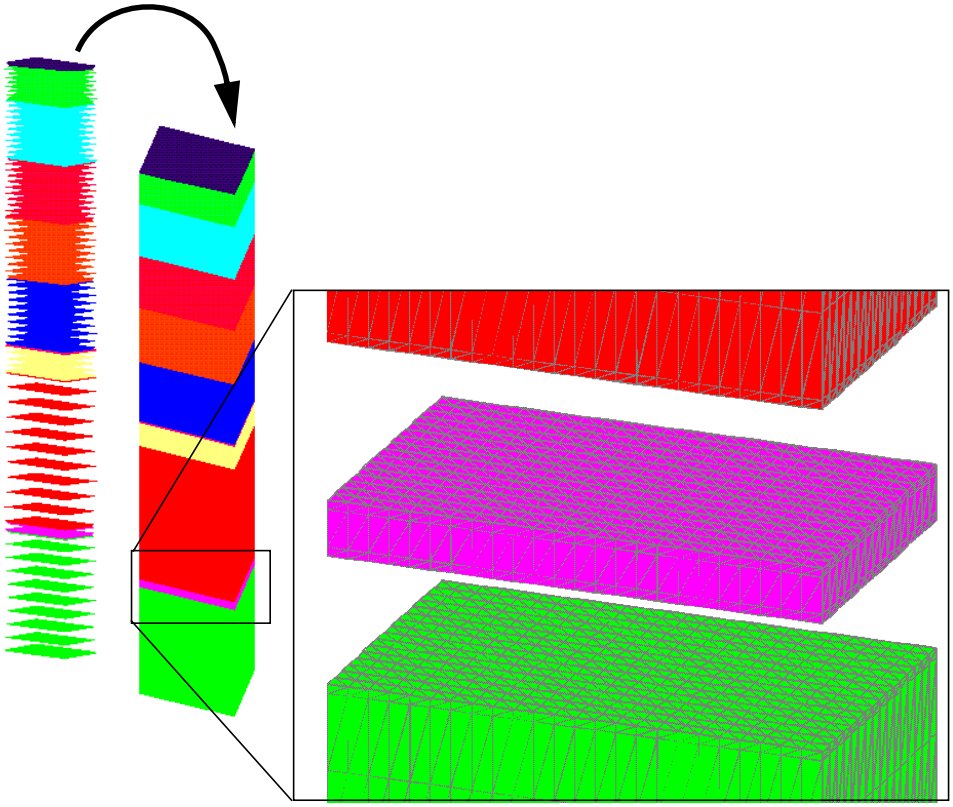

Figure 4-2. The three-dimensional tetrahedral mesh is created from triangulated sheets that are used to create tetrahedral elements stacked atop one another. The enlarged image shows three of the material units in exploded view. Spacing for x and y directions is 1.9 meters, z spacing averages about 2 meters depending on the unit material. A top soil layer was created to a depth of 1.524 meters.

main direction of the gradient. But if the direction of flow is unknown, or known to be non-vertical, the grid may be changed to have no preferential orientation.

To make the grid anisotropic, a smoothing method was applied that allows nodes to move within a material region. The smoothing takes place between iterations of refinement and preferences towards equilateral triangles. This results in edges pointing in random directions, resulting in less grid orientation effects on the solution. The smoothing is combined with refinement called massage. This refinement breaks elements into smaller elements based on a chosen edge length. It also merges points to limit how small an edge can become. Figure 4-4 illustrates this process and shows the resulting grids. The grid with the 65-foot shaft shown in Figure 4-4(c) was used for most of the simulations..

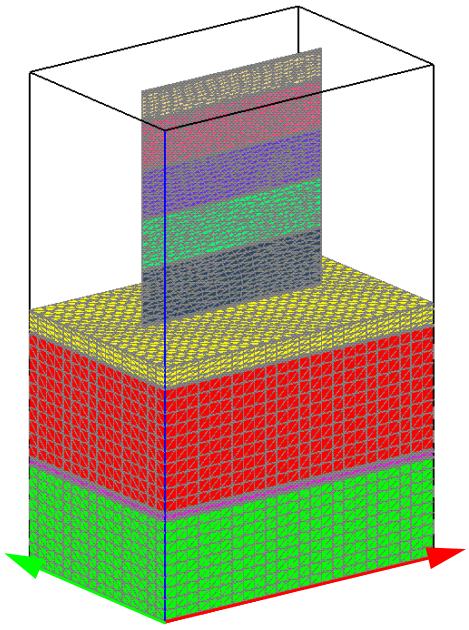

Figure 4-3. Location of extracted slice in reference to the tetrahedral grid. Image is shown with 5x exaggeration in X and Y. The slice was made at y = 535030.68 meters (1755350 feet). Minimum x for the slice is 495497.7350 meters, maximum is 495543.455 meters. The elevations start at 2176 meters and go down to the water table at about 1824 meters.

4.3 BOUNDARY CONDITIONS

4.3.1 Background Flow

The background flow field is set up by applying a steady infiltration rate across the upper boundary of the two-dimensional computational grid. Although the grid is refined around the experimental shaft, the shaft (red area in Figure 4-4(c)) is assigned the hydrologic properties of Unit 4 to simulate background conditions. Three different infiltration rates were run, 0.1 mm/yr, 0.5 mm/yr and 1.0 mm/yr. The lower boundary represents the water table with a fixed saturation of 0.99. The side boundaries allow no flow or transport. The flow fields were run to steady state, and the simulated water content profiles were compared to the background water content data presented in Figures 2-4 and 2-5. The results of these simulations are presented later in this report.

4.3.2 Transient Flow

4.3.2.1 Current Conditions

For the transient flow simulations, we assumed that the site's native conditions were disturbed in 1961 by the addition of the shaft and the asphalt cover. The material properties of

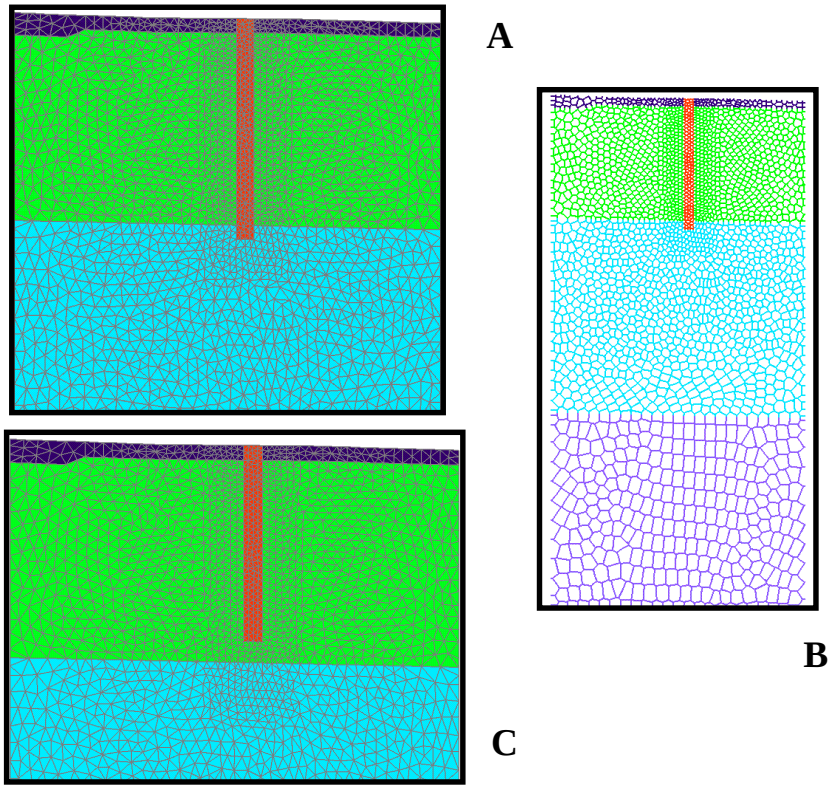

Figure 4-4. This refinement used a massage algorithm which reconnects the grid based on a minimum and maximum edge length. Along with smoothing, this results in a grid with more nodes (4158 nodes and 7955 elements), but a better distribution for calculations. Grid A shows the triangles in the final Delano version of the massaged grid. Image B is the same grid with Voronoi cells shown. Image C shows the same method used on the 65 foot shaft grid which has 4138 nodes and 7916 elements.

crushed tuff were substituted for the Unit 4 properties present in the shaft nodes (red zone in Figure 4-4(c)). Higher infiltration rates were applied along the upper boundary for a period of 39 years to predict the location of contaminants in the year 2000, when monitoring holes are likely to be installed. The steady background flow field was used as an initial condition for the transient runs with the exception that the saturation of the crushed tuff in the shaft was set to 0.167. Five different upper boundary conditions were tested to calibrate the model to observed data, two with a fixed saturation and three with fixed infiltration rates.

For the fixed-saturation boundary, we assumed that the asphalt pad trapped water in the underlying fill and soil creating a near constant saturation of 0.6 to 0.7 at the fill/soil interface. This boundary condition is derived from the shallow moisture data presented in Figure 2-5. If the fill material averages 3 to 3.5 feet thick in these wells, the gravimetric moisture content at the fill/soil interface lies between about 18 and 23%, which is equivalent to a saturation of 0.6 to 0.7.

The fixed-infiltration upper boundary is based on estimates made by Wilson and Kisiel (1998). They calculate a range in subsurface flux rates of 61 to 388 mm/yr before the implementation of any stabilization measures. The lower value results from direct precipitation onto the asphalt pad. They assumed that the precipitation falling on the asphalt pad was channeled through cracks in the asphalt and distributed uniformly in the underlying fill. Their estimates rely on observed crack width, length and spacing and on the hydrologic properties of the fill. The higher value includes contributions from surface water run-on and interflow run-on. Our simulations use rates of 60, 150 and 388 mm/yr to cover their estimated range. These infiltration rates far exceed values in uncovered mesa tops on the Pajarito Plateau and approach values estimated beneath surface impoundments at TA-53 (Rogers et al., 1996) and along the canyon bottom in Los Alamos canyon (Gray, 1995; Robinson et al., 1999).

4.3.2.2 Future Conditions

Predictions were run for an additional 100 years in order to assess the effectiveness of the recent site improvements. These include a set of simulations in which we assume the improvements were not made (i.e., no runon control or surface regrading was performed and the asphalt pad remains) and another set of simulations with the recent changes in place.

4.4 SOURCE TERM

Transport calculations were run for both uranium and cesium at infiltration rates of 60 mm/yr and at 388 mm/yr. Plutonium migration is expected to be bounded by that or uranium (see Section 6.2). We assume that these species were uniformly distributed throughout the fracture zone immediately upon detonation of the HE explosive. The fracture zone was considered to have a diameter of 15 feet. The contaminant source was assumed to be distributed in the pore water contained within this matrix of this fractured volume.

4.4.1 Uranium

We assumed that uranium is transported both as a dissolved species and as colloidal particles. As a dissolved species, uranium was released from the source region at its solubility limit of 2.76×10^{-7} moles/L, based on the speciation calculations presented in Section 2.4.2, throughout the simulation. The solubility limit should be the appropriate source concentration for most of the

detonation experiments that contained uranium. For the colloid simulations, we assumed an initial source of 1 kg of colloids in a size range that can be transported through the matrix pores. This result will requiring scaling based on the actual uranium inventory in a particular shaft and on the fraction of colloids that are mobile in the porous medium.

4.4.2 Cesium

Cesium is assumed to be transported as a dissolved species with infinite solubility. Therefore, we assumed that the entire mass of cesium was immediately available for transport. Again, we used an initial source of 1 kg of cesium distributed in the matrix pore water located throughout the initial fracture volume. This result can be scaled by the true contaminant inventory in a shaft.

5.0 - RESULTS AND DISCUSSION

5.1 UNSATURATED-ZONE FLOW

5.1.1 BACKGROUND FLOW

Figures 5-1 and 5-2 shows the simulated, background moisture profiles compared to site data to depths of 120 feet and 700 feet, respectively. The simulated 0.1-mm/yr profile appears to match the site data very well, and this infiltration rate was chosen as the background condition. The failure to capture the moisture spike at about the 400-foot depth (Fig. 5-2) indicates a need for more accurate hydrologic properties along the vapor-phase notch (Fig. 2-1).

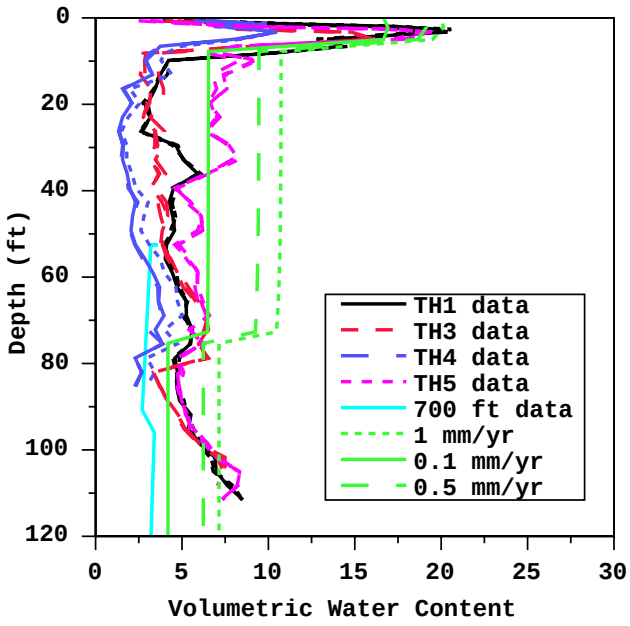

Figure 5-1. Comparison of simulated water content profiles (green) for steady infiltration at 0.1, 0.5 and 1.0 mm/yr to site data from various boreholes surrounding the asphalt pad area, which represent background flow conditions to 120 feet.

5.1.2 TRANSIENT FLOW AT AREA 2

5.1.2.1 Current Conditions

Figure 5-3 compares simulated moisture profiles to site data collected from beneath that asphalt pad in holes 49-2906 and 49-2907 in February, 1994. The moisture profiles predicted by fixing the soil saturation at 0.6 and 0.7 bound the data. A fixed saturation of 0.63 to 0.65 would

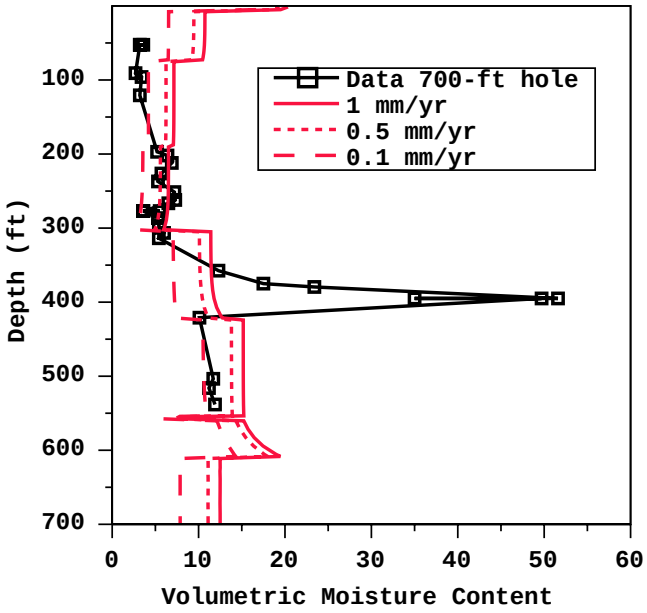

Figure 5-2. Comparison of simulated water content profiles (red) for steady infiltration at 0.1, 0.5 and 1.0 mm/yr to site data (black) from hole 49-2901, which represents background flow conditions to 700 feet.

probably fit the moisture data well and be based on site data. The 60-mm/yr infiltration rate predicted by Wilson and Kisiel (1998) matches the data very well. The infiltrating moisture front penetrates to a depth of about 65 feet in both the simulation and in these two data sets. The higher rates, 150 mm/yr and 388 mm/yr, overpredict water contents as well as the penetration depth of the water during the enhanced recharge period. Therefore, we assumed that the 60-mm/yr rate represents the average flow rate beneath the asphalt pad away from Shaft 2-M and CH-2. Also, a matrix flow model controlled by infiltration from the surface appears to adequately fit these data.

Figure 5-4 compares simulated moisture profiles to moisture data collected in July, 1998, from CH-2. In this case, the simulated results do not match the data particularly well, probably because a steady-infiltration, upper boundary condition does not describe the history of water addition in this area. As mentioned in Section 2.3.1, this hole received large volumes of water during drilling and following the subsidence of the asphalt over the neighboring shaft 2-M. The hole was filled with water to a depth of 50 feet for a year following the subsidence event and to a depth of 150 feet for over two years in the late 1970's. We postulate that the increased moisture content in CH-2 is largely affected by a few transient events that are not typical of the majority of the area under the asphalt pad. This profile does not have the obvious infiltration front seen in the data from the other two boreholes beneath the pad (Figure 2-1). Interestingly, the moisture

increases in the lower 150 feet of the hole. This increase may be the result of water loss from the borehole annulus to the surrounding formation. Although CH-2 was cased, the integrity of the seal some 40 years after its emplacement is questionable (Farley, pers comm, 1999).

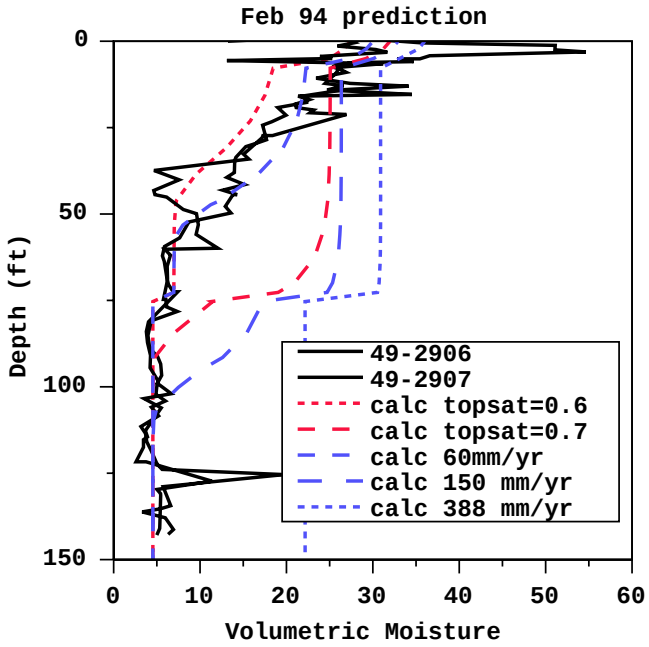

Figure 5-3. Comparison of simulated water content profiles to site data (black) collected in February, 1994, from two boreholes located beneath the asphalt pad. The red curves show results for simulations with fixed saturations of 0.6 and 0.7 in the soil beneath the pad. The blue curves show results for simulations with fixed infiltration rates of 60, 150 and 388 mm/yr.

The simulated 388-mm/yr moisture profile is considered to be a conservative estimate for the upper 300 feet of the profile and is used as an upper bound for the transport calculations that follow. We explain the high moisture content in the lower 150 feet as a direct loss of water from the borehole to the formation. Interestingly, in 1980 the standing water in the borehole did not decrease with time and was eventually bailed. This observation is evidence that even with a standing head of water, percolation is very slow.

Figure 5-5 (a) and (b) show the saturation fields throughout the unsaturated zone that result from the steady, background flow rate of 0.1 mm/yr and for an increased infiltration rate of 60 mm/yr for the 39-year period from 1961 through 2000, respectively. By comparing these two figures, we see that the increased flow yields an increase in calculated saturation only for the soil layer (from about 0.4 to about 0.8) and in Unit 4 (from about 0.15 to about 0.50). The saturation values

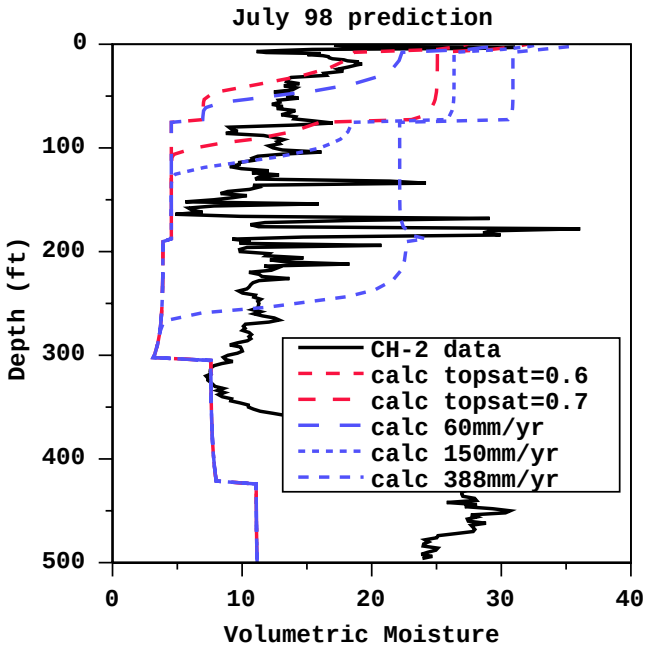

Figure 5-4. Comparison of simulated water content profiles to site data from CH-2 (black) collected in July, 1998, beneath the asphalt pad. The red curves show results for simulations with fixed saturations of 0.6 and 0.7 in the fill beneath the pad. The blue curves show results for simulations with fixed infiltration rates of 60, 150 and 388 mm/yr.

for the remainder of the unsaturated zone (below Unit 4) remain very close to their background values.

Figure 5-6 (a) and (b) show the simulated, unsaturated-zone saturation fields from the steady, background flow rate of 0.1 mm/yr and for an increased infiltration rate of 388 mm/yr for the 39-year period, 1961 through 2000). The saturation front proceeds much further over 39 years at the higher flow rate (388 mm/yr) than at 60 mm/yr. We see that for this case, the increased flow yields an increase in saturation down through Unit 2. Below Unit 2, the saturation values remain near their background values.

5.1.2.2 Future Conditions

To assess the results of the recent site improvements, we performed flow simulations for an additional 100 years into the future, to the year 2100. With these simulations, we compare the saturation profiles that result if no site improvements had been made (i.e., the infiltration rate remains at either 60 mm/yr or 388 mm/yr) to the profiles that result if the site returns to its native condition (0.1 mm/yr). Figures 5-5 (c) and (d) show the resulting saturation fields for the year 2100 when the initial 39-year infiltration rate of 60 mm/yr was followed by an additional 100 years of

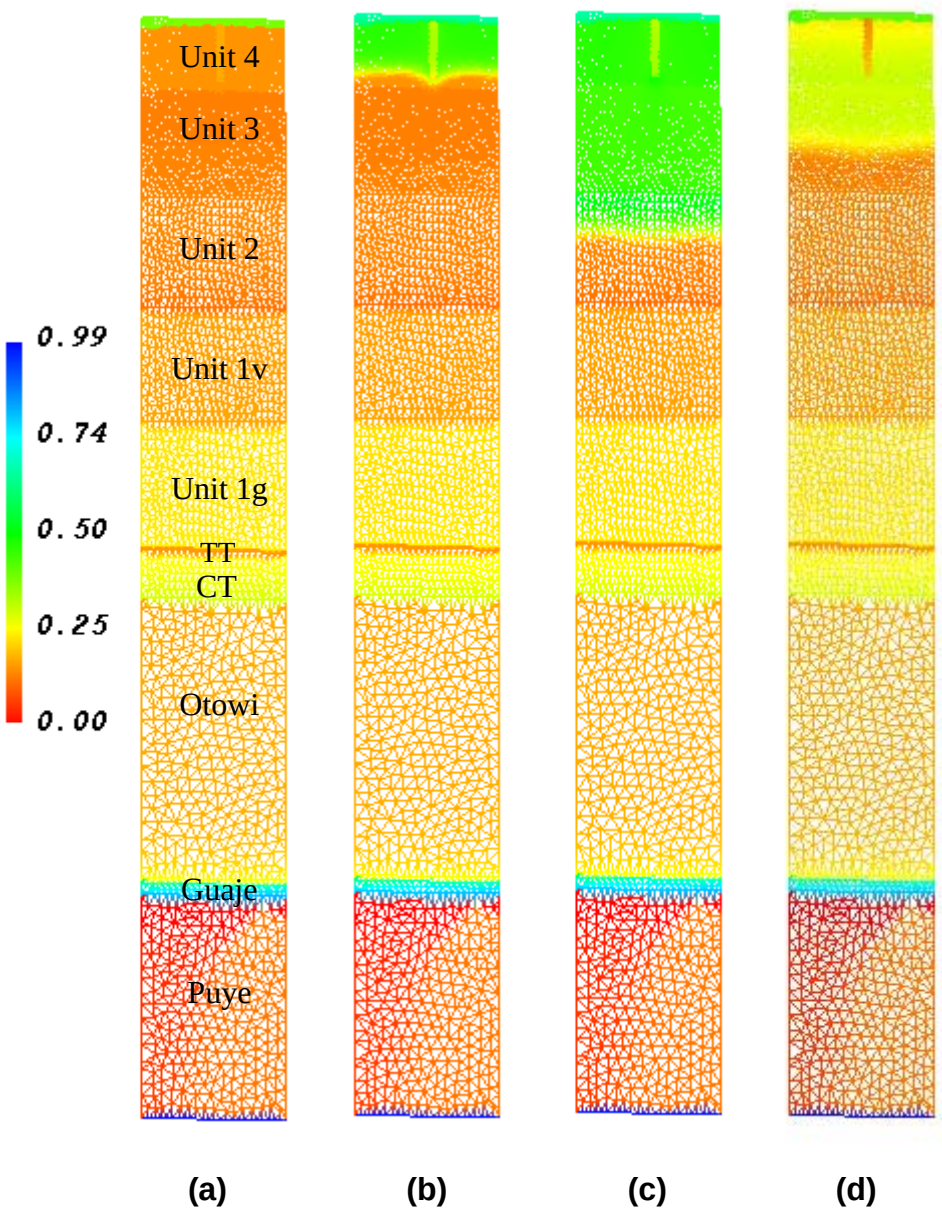

Figure 5-5. Simulated saturations for the entire unsaturated zone (a) background flow field at 0.1 mm/yr, (b) current condition with recharge of 60 mm/yr since 1961, (c) condition in 100 years if recharge continues at 60 mm/yr and (d) condition in 100 years if recharge returns to background rate of 0.1 mm/yr

either 60 mm/yr (Fig. 5-5 (c)) or 0.1 mm/yr (Fig. 5-5 (d)). If infiltration remains at 60 mm/yr, the moisture front advances into Unit 2. However, if infiltration at the site returns to its native condition, the moisture that accumulated over the 39-year period of higher percolation is

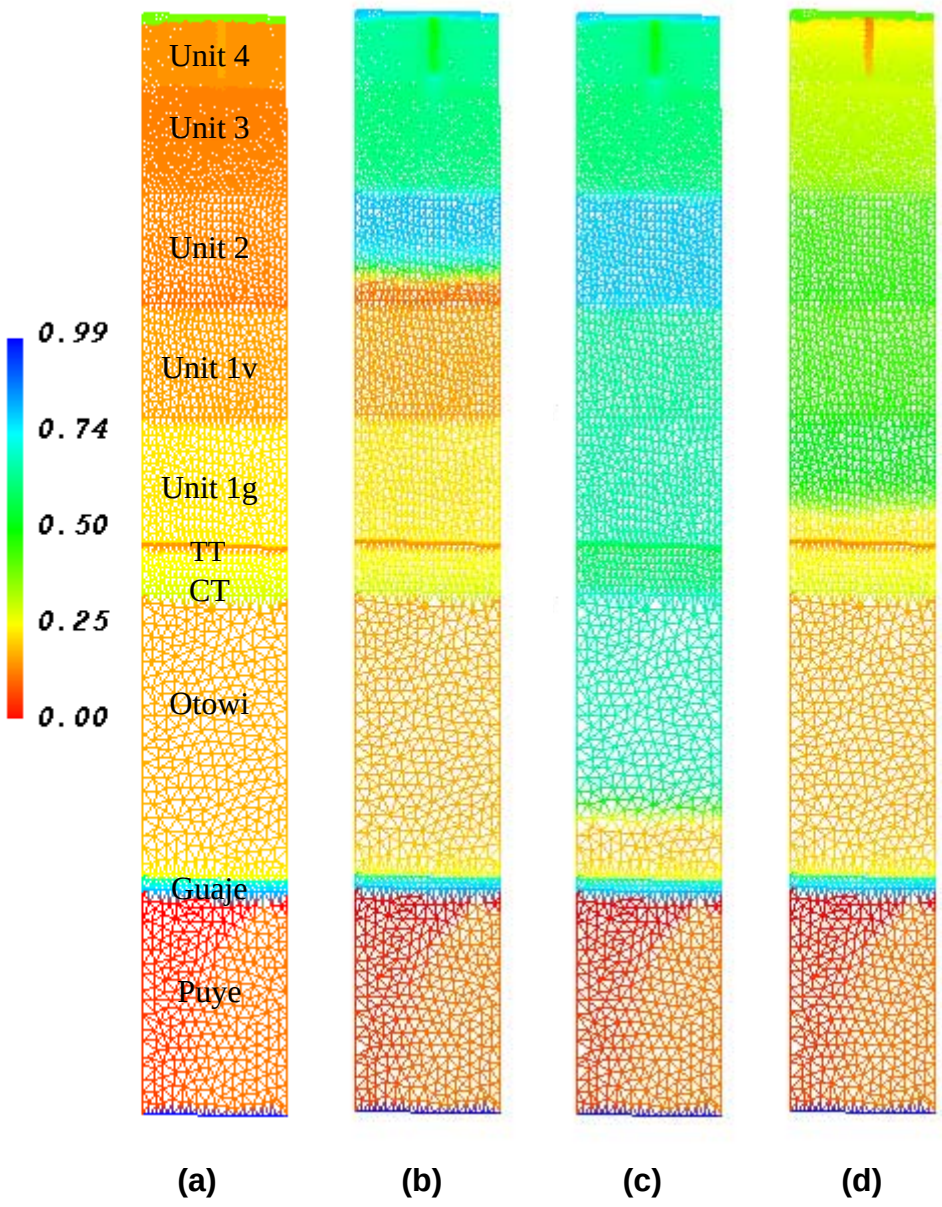

Figure 5-6. Simulated saturations for the entire unsaturated zone (a) background flow field at 0.1 mm/yr, (b) current condition with recharge of 388 mm/yr since 1961, (c) condition in 100 years if recharge continues at 388 mm/yr and (d) condition in 100 years if recharge returns to background rate of 0.1 mm/yr

redistributed throughout the soil layer and Units 3 and 4. The soil, Unit 4 and the shaft are predicted to dry out considerably over the next 100 years because of the site improvements.

Figures 5-7 (a) and (b) show the predicted evolution of insitu saturation at four subsurface locations, assuming that the infiltration rate returned from 60 mm/yr to 0.1 mm/yr after the removal of the asphalt pad. Both the soil and the crushed tuff dry considerably over the first five to seven years. In Unit 4, the saturation increases slightly during this same time period as water drains downward from the soil. This increase may be an artifact of the boundary condition used for the soil/water interface rather than a true phenomenon. The model only accounts for decreased infiltration and does not account for evapotranspiration at the surface. Soil moisture may decrease more in response to evapotranspiration than as a result of moisture redistribution to deeper units. In Unit 3, virtually no saturation change occurs during the first 25 years. Then between 25 and 75 years, the saturation rises sharply as the moisture front relaxes and moves deeper into the subsurface. Evapotranspiration should have a negligible effect on moisture in the deeper units.

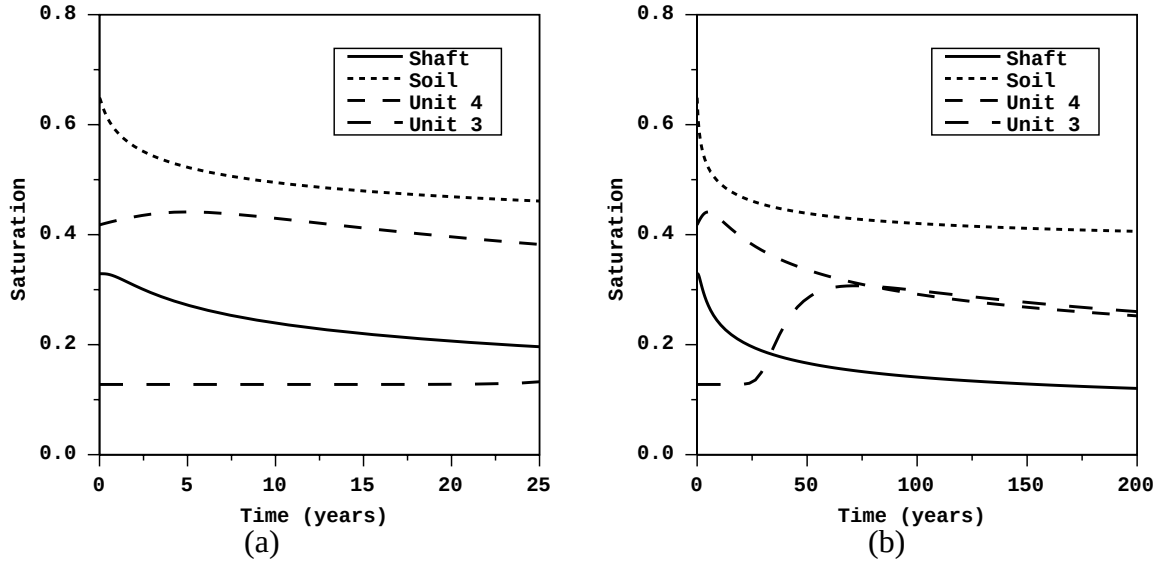

Figure 5-7. Predicted evolution of saturation resulting from the recent site improvements (assuming flow returns from 60 mm/yr to 0.1 mm/yr) at four subsurface locations (a) short term and (b) longer term.

Figures 5-6 (c) and (d) show the resulting saturation fields for the year 2100 when the initial 39-year infiltration rate of 388 mm/yr was followed by an additional 100 years of either 388 mm/yr (Fig. 5-6 (c)) or 0.1 mm/yr (Fig. 5-6 (d)). If infiltration remains at 388 mm/yr, the moisture front advances well into the Otowi Member with saturation values ranging from about 0.5 to 0.8 to that depth. Even if infiltration returns to the background value, the moisture that accumulated over the initial 39-year period of higher percolation is redistributed down through Unit 1g, increasing

saturations up to 0.5 in Units 2, 1g and 1v. However, the soil, the shaft, and Units 3 and 4 again are predicted to dry considerably at the background flow rate.

5.1.3 Flow at Areas 2A and 2B

No numerical simulations were performed for Areas 2A and 2B because we did not feel that the moisture data from the shafts or the information concerning the ponded boundary condition were sufficient to either calibrate or develop a flow model. Therefore, this discussion is based only on the shaft moisture data (Fig. 2-9) and the simulations performed for Area 2. We would expect a higher infiltration rate in Area 2A than the portion of Area 2B near Shaft 2B-Y. However, the moisture measured in Shaft 2B-Y lies between that in Shafts 2A-Y and 2A-O indicating that infiltration at these two areas is similar. We should note that both the fill and the packing of these three shafts may differ.

If we compare the moisture measured in the shafts (Fig. 2-9) to the saturation calculated for the shafts beneath the asphalt pad (Fig. 5-7), it seems that the shafts surrounding the asphalt pad are dryer than those beneath the pad implying that infiltration beneath the pad is higher than in the adjacent, periodically ponded area. (Note that if the shaft saturation shown in Figure 5-7 is given in terms of moisture content, it ranges from a high at time zero of around 15% to a low of around 7% at 200 years.) This statement requires a strong qualification. The simulations assume that the shafts are filled with crushed tuff with properties similar to Unit 2 crushed tuff from MDA G. If the fill is crushed tuff, it is likely that the material is from Unit 4 as that is the material that was excavated to install the shafts. Also, some documents state that the shafts are filled with sand. Either of these materials could have hydrologic properties that are significantly different than those for Unit 2 crushed tuff. In that case, the data and the simulations could differ significantly. Our conclusion that the data indicate lower infiltration in the ponded area than beneath the asphalt pad would then be mistaken.

5.2 CONTAMINANT TRANSPORT

5.2.1 Current Conditions

Transport calculations of dissolved uranium, dissolved cesium and colloidal particles were run for a simulation time of 39 years with the transient flow fields presented in Section 5.1.2.1.

Figures 5-8 show the simulated results for the current locations and concentrations of these contaminants, assuming the two transient infiltration rates of 60 mm/yr and 388 mm/yr. In Figures 5-8 (a), (c), and (e), the contaminants are located mainly within the original fractured volume. This implies that virtually no migration of either dissolved or colloidal uranium or of dissolved cesium has occurred from the shafts in Area 2 over the past 39 years if the 60-mm/yr infiltration rate adequately describes the water flow beneath the asphalt pad during its life-time at the site. The migration is controlled by the advance of the wetting front, which for the 60-mm/yr case has only advanced through Unit 4 (Fig. 5-5 (d)). The cesium also remains within the original fractured volume at the 388 mm/yr flow rate (Fig. 5-8 (d)) because of its very high Kd.

The dissolved and colloidal uranium do migrate at the 388 mm/yr infiltration rate. The dissolved uranium plume (Fig. 5-8 (b)) has spread from its original diameter of 15 feet to about 40 feet. The colloidal particles (Fig. 5-8 (f)) advance the farthest. Because the wetting front has traveled into Unit 2 at this higher infiltration rate, the non-sorbing colloids also migrate into this layer.

If the transported mass of uranium is compared to the mass of uranium in the shafts, we can roughly estimate the fraction of uranium that remains within the source region. From Table 2-1, we see that there are about 100 kg of uranium in Area 2. For illustrative purposes, let’s assume that a shaft has on the order of 10 kg or about 40 moles of uranium. For the FEHM simulations of dissolved uranium, only small quantities of uranium dissolve over the 39-year time period - 0.02 moles at the 60 mm/yr flow rate and 0.05 moles at the 388 mm/yr flow rate. The solubility-limited source term holds for any uranium-contaminated shaft provided that the mass of uranium is large enough to generate a solubility-limited concentration. Therefore, the concentrations shown in Figures 5-8 (a) and (b) represent values that are likely to be seen in the field. With these assumptions, the simulations predict that about 0.1% or less of the uranium has dissolved over the 39 years since the source was emplaced.

To predict the mass of colloids that can readily transport, the particle-size distribution is compared to the water-filled pore size. For the 60 mm/yr flow rate, the saturation in Unit 4 reaches about 50% (Fig. 5-5 (b)) in the year 2000 and is much drier below that unit. Figure 2-10 shows that this corresponds to a maximum pore size of 0.11 microns in the Topopah Spring tuff and 0.06 microns in the Calico Hills tuff. For the 388 mm/yr flow rate, the saturation is about 65% in Units

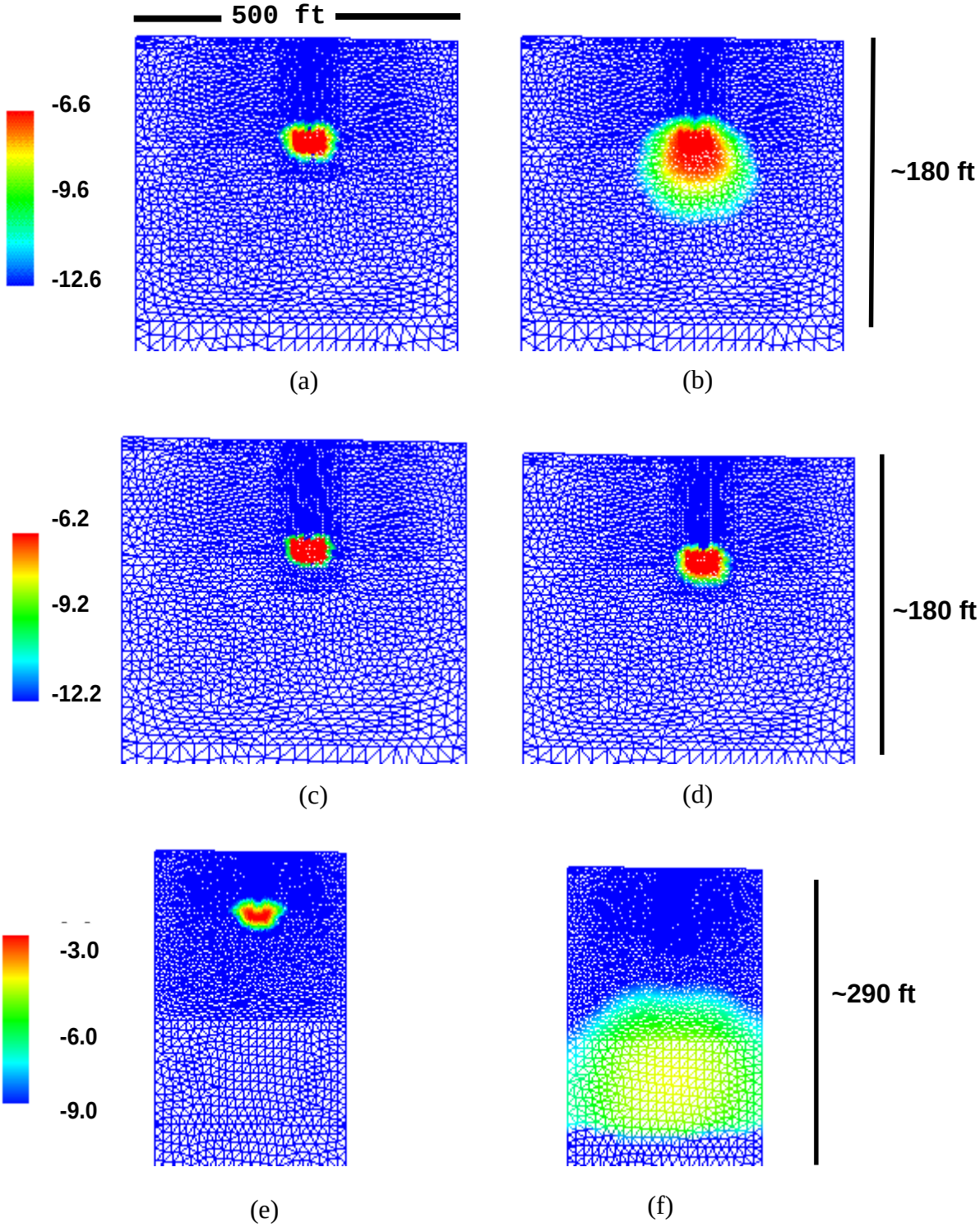

Figure 5-8. Contour plots of concentration [log scale] for (a) dissolved uranium at 60 mm/yr, (b) dissolved uranium at 388 mm/yr, (c) dissolved cesium at 60 mm/yr, (d) dissolved cesium at 388 mm/yr, (e) colloids at 60 mm/yr, and (f) colloids at 388 mm/yr.

3 and 4 in the year 2000 (Fig. 5-6 (b)). This corresponds to maximum pore sizes of 0.50 microns and 0.08 microns in the Topopah Spring and Calico Hills tuff, respectively. If pore sizes are similar in the Bandelier tuffs, then only particles less than 0.50 microns should be mobile in the tuff matrix. Next, the particle-size distribution in Figure 2-3 shows that approximately 1% of the particles are 0.50 microns or less. Therefore, at most 1% of the particles should be mobile behind the moisture front. The concentration of colloids does depend on the source term. Therefore, the concentrations in Figures 5-8 (e) and (f) must be scaled by 1% of the actual uranium source to determine the expected field concentrations. Considering both uranium sources (solubility limited and colloids), the total mass of uranium that is available for transport is only about 1% of the total uranium mass.

5.2.2 Future Conditions

Figures 5-9 show 100-year predictions for the soluble uranium plumes with and without the implementation of the recent BMPs, assuming an initial (from 1961through 2000) infiltration rate of 60 mm/yr. These simulations begin with the plume shown in Figure 5-8 (a) and the saturation distribution shown in Figure 5-5 (b). A continuous, constant concentration of uranium, controlled by its solubility limit, is generated in the source region throughout the simulation. Figure 5-9 (a) shows the resulting plume if the infiltration rate returns to the background value of 0.1 mm/yr (corresponding to the saturation field in Figure 5-5 (d)). Although the infiltration rate in this simulation has returned to the background value (0.1 mm/yr), the plume spreads into Unit 3. Therefore, uranium migration is further during this 100 years than during the first 39 years at the enhanced infiltration rate (60 mm/yr) because of moisture redistribution (compare Fig. 5-5 (b) and (d)). Figure 5-9 (b) shows the plume that would result if the infiltration rate had remained at 60 mm/yr (corresponding to the saturation field in Figure 5-5 (c)).

With either boundary condition, the simulations indicate that the soluble uranium plume should not migrate much further over the next 100 years. Considering mass balance arguments similar to those made in Section 5.2.1, FEHM indicates that only 0.024 moles of uranium would dissolve over the entire 139-year time frame if infiltration returns to the background value. If infiltration remains at 60 mm/yr, 0.034 moles would become soluble. These totals still amount to less than 0.1% of the uranium source.

Future predictions for cesium were not run. However, based on its high Kd value, cesium would migrate even less than dissolved uranium.

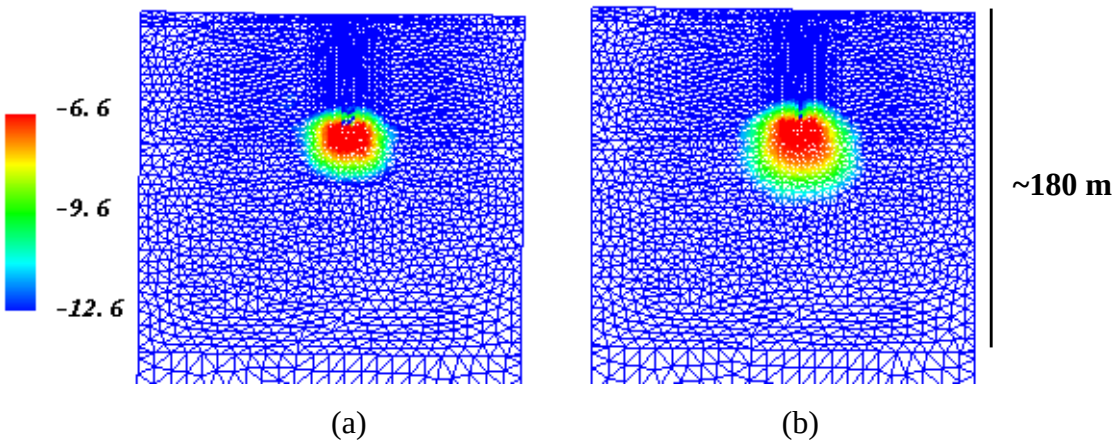

Figure 5-9. Predictions of dissolved uranium transport (log-scale concentration) from Area 2 100 years into the future (2100) with and without the recent site improvements (a) infiltration returning from 60 mm/yr to 0.1 mm/yr and (b) infiltration remaining constant at 60 mm/yr.

Figures 5-10 (a) through (d) show future predictions of colloidal uranium transport with and without the recent site improvements for both the 60 mm/yr and the 388 mm/yr infiltration rates. The simulations shown in Figures 5-10 (a) and (b) are a continuation of the 60 mm/yr colloid simulation. They use the plume shown in Figure 5-8 (e) and the saturation distribution shown in Figures 5-5 (b) as initial conditions. Then, either 0.1 mm/yr or 60 mm/yr of infiltration is applied for the 100-year simulation. No additional colloids are supplied because the colloid source is assumed to be formed by the initial explosion and not regenerated. The simulations indicate that if flow returns to 0.1 mm/yr, the colloids migrate into Unit 3. If flow remains at 60 mm/yr, the colloids migrate into Unit 2.

The simulations shown in Figures 5-10 (c) and (d) are a continuation of the 388 mm/yr colloid simulation. For these, the plume in Figure 5-8 (f) and the saturation distribution in Figure 5-6 (b) are the initial conditions. Then, either 0.1 mm/yr or 388 mm/yr of infiltration is applied for the 100-year simulation. Again, no additional colloids are generated during the simulation. The colloids migrate much further in these simulations because of water redistribution. If flow returns to 0.1 mm/yr, the colloids migrate into Unit 1g, while if flow remains at 388 mm/yr, the colloids migrate into the Otowi Member. Since no additional colloids are added during this phase of the simulation, the mass balance arguments are identical to those discussed for colloids in Section 5.2.1 (i.e., no more than 1% of the mass of uranium should be available for transport as colloids).

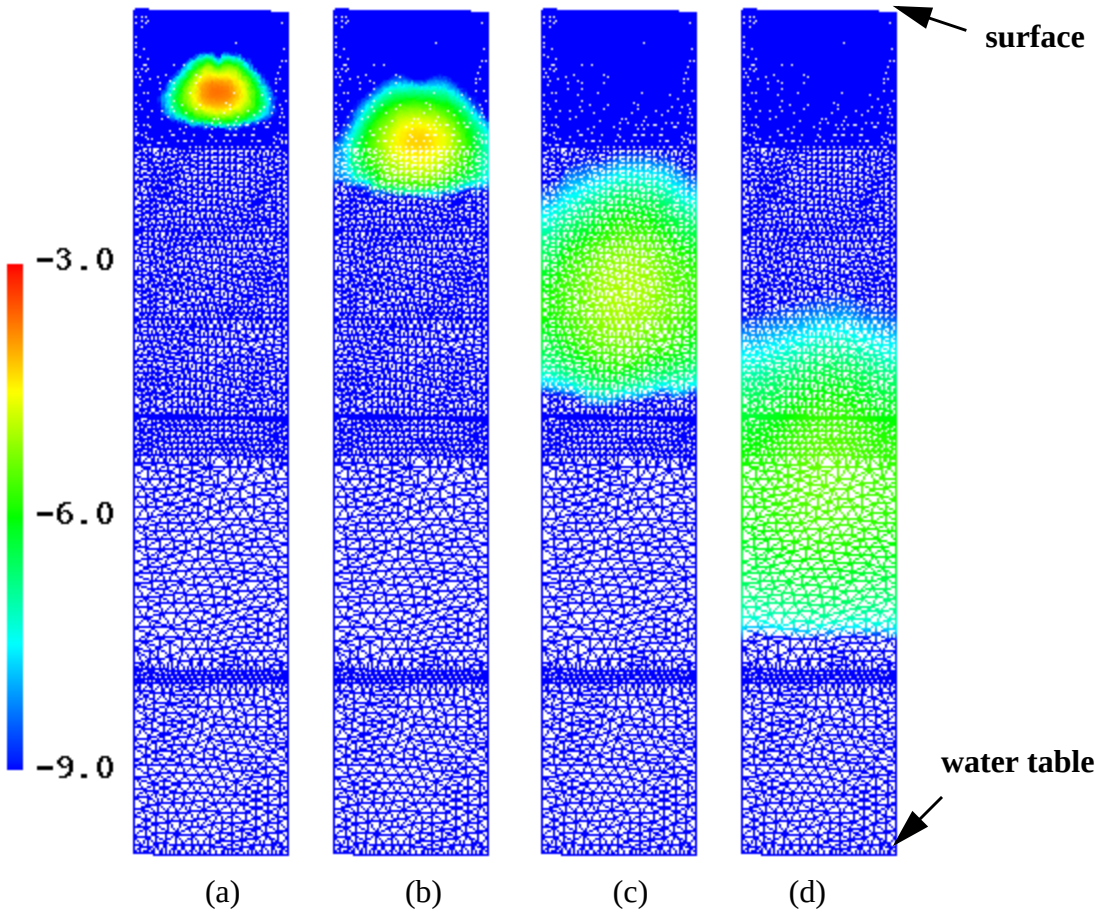

Figure 5-10. Predictions of transport from Area 2 100 years into the future (2100) with and without the recent site improvements for uranium colloids (a) flow returning from 60 mm/yr to 0.1 mm/yr, (b) flow remaining constant at 60 mm/yr, (c) flow returning from 388 mm/yr to 0.1 mm/yr, and (d) flow remaining at 388 mm/yr.

6.0 - CONCLUSIONS

Numerical simulations were used to predict the present-day and future migration of moisture and radionuclides at Area 2 of MDA AB, TA-49. The data and the model support the hypothesis that the installation of the asphalt pad at the site in 1961 resulted in increased subsurface flow which was detrimental to performance. The model also supports the hypothesis that the recent removal of the asphalt pad and other site improvements will lead to less recharge at the site, resulting in lower recharge, dryer subsurface conditions and slower contaminant migration rates. This hypothesis should be confirmed through long-term moisture monitoring, but the monitoring program must be carefully designed to assure meaningful results. Transport simulations indicate that very little contamination has left the source region. This result should also be verified with carefully planned field testing.

6.1 FLOW AT AREA 2

Recharge beneath the pad increased from a low background value near 0.1 mm/yr to higher values comparable to those seen in canyons or beneath surface impoundments. While the asphalt pad was in place, we believe that the 60 mm/yr rate and matrix-dominated flow adequately predict the moisture profile beneath most of the pad because the asphalt prevented large moisture pulses from entering the subsurface. This is supported by the good match between the model and the data in holes 49-2907 and 49-2906 (Fig. 5-3). However, these assumptions may not describe the flow in the area near Shaft 2-M and Corehole-2 where several transient events were observed, and the moisture profile does not indicate steady infiltration of a moisture front. The higher recharge value of 388 mm/yr better fits the data (Fig. 5-4), and we assumed this value may apply to a few shafts local to this area.

The interpretation of the moisture profiles required transient simulations because the penetration depth of the moisture front at this site does not reach the water table (Figures 5-5 and 5-6). Transient analysis provides a sensitive means for estimating recharge when a site is disturbed by predicting the location of the moisture front. Transient analysis was also required to predict the return of the site toward background conditions, which can be quite slow when a large volume of water is redistributed through the unsaturated zone. A jump in infiltration from 0.1 to 60 mm/yr

represents a 600-fold increase or over 23,000 years worth of moisture in a 39-year period. Based on this simplified argument, the slow return of the site to background conditions is not surprising. The simulations predict that measurable changes in moisture may only occur in the soil and the shaft over the next five to ten years.

6.2 TRANSPORT AT AREA 2

The simulations predict that most of the contaminants (~99%) currently remain within the original fractured volume created by the underground explosion. Cesium remains because it sorbs onto the rock matrix. The migration of uranium is limited because its source term consists of particles that are generally much larger than the matrix pore size and also because uranium's solubility is low. Only those uranium particles (colloids) that are smaller than the water-filled pores and the small quantity of dissolved uranium can migrate. The soluble form remains close to the source region because it adsorbs to the local tuff. At the 60 mm/yr infiltration rate, the colloidal uranium should be located very near the original source region. At the highest infiltration rate, which we believe may apply near CH-2, the uranium colloids may have traveled as far as Unit 2. The simulations predict that the site improvements made during 1998 will slow the progression of nuclide migration downward through the vadose zone.

This analysis is based on data that are not site specific. The pore-size distributions are for Yucca Mountain tuffs and the particle-size distribution is from an atmospheric test. Although we believe that these distributions should be similar to those for local conditions, if more site specific data become available, the confidence in these simulations will be higher.

The migration of plutonium should be similar to that of uranium. Data from the MDA G PA indicate that plutonium has a slightly lower solubility than uranium and a higher Kd of about 4 (Longmire et al., 1996, Krier et al., 1997). Also, the atmospheric test data show that plutonium forms fairly large particles that are generally larger than tuff pore sizes (Shreve and Thomas, 1965).

6.3 FLOW AND TRANSPORT AT AREAS 2A AND 2B

Comparison of the moisture data from shafts in Areas 2A and 2B to the simulation data indicate that infiltration in these areas was less than in Area 2, while the pad was in place. If the infiltration rate is lower, then the contaminants in these areas should have migrated even less than in Area 2. This analysis relies heavily on the hydrologic properties of the fill in the shafts, which is unknown.

7.0 - RECOMMENDATIONS

Several recommendations can be made based on this modeling work both for the site itself and for other waste sites around the laboratory.

7.1 AREAS 2, 2A, AND 2B AT TA-49

7.1.1 Data Needs

Site-specific distributions for the pore-sizes of the upper tuff units should be obtained to support the colloid transport model of this site. Also, if information can be found in historic laboratory reports describing particle-size distributions for underground experiments involving both high explosives and special nuclear materials, this information would decrease the uncertainty of the colloidal source term for the site.

To predict flow in Areas 2A and 2B, the hydrologic properties of the fill used in the shafts are key parameters. These data should be measured. Also, deep moisture measurements in Area 2A would allow the calibration of a flow model.

7.1.2 Field Testing and Monitoring

The installation of two experimental boreholes is proposed for this site: a subvertical borehole beneath Area 2 to determine the extent of the contaminant plume, and an extension of the borehole through Shaft 2A-O to determine the extent of the moisture front beneath Area 2A. Care should be taken during the construction and completion of the boreholes and during monitoring activites so that the boreholes do not provide a conduit for the enhanced migration of contaminants at the site.

We recommend that the subvertical borehole be carefully placed within close proximity to the expected fractured zone beneath at least one shaft. This will verify that most of the contamination actually remains near the source region. The shaft should angle down no further than Unit 2. Sample collection and analysis should be designed to determine the presence and size range of contaminant-bearing colloidal particles. Modeling results should be coupled with experimental constraints to determine optimum borehole placement.

We recommend that the vertical borehole through Shaft 2A-O extend to 150 feet to determine the moisture profile beneath Area 2A. We do not expect that the moisture profile in this area is much deeper than that in Area 2 based on the limited moisture data collected in the two shafts in Area 2A. The extension of the borehole to 150 feet will provide a good data set to compare to those collected in hole 49-2906 and 49-2907 located within Area 2, which adequately capture the moisture profile in that region.

We recommend that moisture monitoring at the site be carefully planned to yield unambiguous results. Over the next five to ten years, moisture fluctuations within Unit 3 or below the center of Unit 4 are likely to be very slow. Monitoring in the soil or at a shallow location in Unit 4 should give more meaningful results.

7.1.3 Future Modeling

These results are based on very little site data. As additional moisture monitoring and contaminant concentrations are measured in the field, both the conceptual and the numerical models will be revised to better fit the field data. Also, modeling can be a key component of experimental design to assure that meaningful data are collected in both field and laboratory tests.

7.2 OTHER LABORATORY SITES

7.2.1 Asphalt Placement

The placement of asphalt at other waste disposal facilities around the laboratory should be questioned. Calibration of the flow model to field data at this site indicate that the asphalt caused an increase in percolation from a background value of near 0.1 mm/yr to a value close to 60 mm/yr, which is similar to percolation rates seen in canyons. This represents a 600-fold increase, which is an undesirable change in terms of the long-term performance of a waste site. Transient flow models may need to be used to interpret moisture profiles at laboratory sites that have had significant surface disturbances.

7.2.2 Hydrologic data

Hydrologic properties from TA-49 will be compared to site-wide data to revise the average property values and to determine if mean property values around the Pajarito Plateau are representative of TA-49 hydrologic conditions.

8.0 - ACKNOWLEDGEMENTS

The authors would like to thank the following individuals for their assistance: Tom Kunkle provided technical understanding and information that led to our understanding of the source term at this site. Dwain Farley and Charlie Wilson provided expert insight into the history and the hydrology of the site. Maureen McGraw suggested the approach that was used to understand colloid transport at the site. Bruce Robinson suggested including a discussion of moisture monitoring at the site and also performed a technical review of the document. Greg Cole provided stratigraphic surfaces used in grid generation. Everett Springer supplied the hydrologic properties for the site. Brent Newman provided moisture and soils data for the site. Jack Nyhan provided moisture data for the site. Phil Stauffer and Diana Hollis also reviewed the document.

9.0 - REFERENCES

OU 1144 RFI Work Plan (1992). Los Alamos National Laboratory document LA-UR-92-900.

Birdsell, K.H., W.E. Soll, K.M. Bower, A.V. Wolfsberg, T. Orr, T.A. Cherry, (1997). "Simulations of Groundwater Flow and Radionuclide Transport in the Vadose and Saturated Zones Beneath Area G, Los Alamos National Laboratory," Los Alamos National Laboratory manuscript LA-13299-MS.

Brandes, D., (1998). "A Low-Dimensional Dynamical Model of Hillslope Soil Moisture, with Application to a Semiarid Field Site," PhD Dissertation, Pennsylvania State.

Davenport, D.W. (1996). "Summary of Soil Characterization, TA-49, Area 2-A", memo to B. Wilcox and J. Nyhan.

Environmental Protection Agency (2000). "Region 6 Corrective Action Strategy, Guide for Pilot Projects" EPA document.

Gable, C.W., T. Cherry, H. Trease, and G.A. Zyvoloski, (1995). "GEOMESH Grid Generation," Los Alamos National Laboratory document LA-UR-95-4143.

Gray R.N., (1995). "Hydrologic Budget Analysis and Numerical Simulations of Groundwater Flow in Los Alamos Canyon near Los Alamos, New Mexico," Master's Thesis, University of New Mexico, Albuquerque, NM.

Hollis, D., E. Vold, R. Shuman, K. Birdsell, K. Bower, W. Hansen, D. Krier, P. Longmire, B. Newman, D. Rogers, and E. Springer, (1997). "Performance Assessment and Composite Analysis for the Los Alamos National Laboratory Disposal Area G," Los Alamos National Laboratory document LA-UR-97-85, Report-54G-013.

Krier, D., P. Longmire, R.H. Gilkeson, and H.J. Turin, (1997). "Geologic, Geohydrologic and Geochemical Data Summary of MDA G, TA-54 Los Alamos National Laboratory," Los Alamos National Laboratory document LA-UR-95-2696.

Longmire, P., C.R. Cotter, I.R. Triay, J.J. Kitten, C. Hall, J. Bentley, D. Hollis, and A.I. Adams, (1996). "Batch Sorption Results for Americium, Neptunium, Plutonium, Technetium, and Uranium Transport through the Bandelier Tuff, Los Alamos, New Mexico," Los Alamos National Laboratory document LA-UR-96-4716.

Purtymun, W.D., (1995). "Geologic and Hydrologic Records of Observation Wells, Test Holes, Test Wells, Supply Wells, Springs, and Surface Water Stations in the Los Alamos Area," Los Alamos National Laboratory manuscript LA-12883-MS.

Purtymun, W.D., (1984). "Hydrologic Characteristics of the Main Aquifer in the Los Alamos Area: Development of Groundwater Supplies," Los Alamos National Laboratory manuscript LA-9957-MS.

Robinson, B.A., M. Witkowski, C.J. Elliot, L. Dale, R. Koch, (1999). "Numerical Model of Flow and Transport for Los Alamos Canyon," Los Alamos National Laboratory Environmental Restoration Project Milestone.

Rogers, D.B., and B.M. Gallaher, (1995). “The Unsaturated Hydraulic Characteristics of the Bandelier Tuff,” Los Alamos National Laboratory manuscript LA-12968-MS.

Rogers, D.B., B.M. Gallaher, and E. Vold, (1996). “Vadose Zone Infiltration Beneath the Pajarito Plateau at Los Alamos National Laboratory,” Los Alamos National Laboratory document LA-UR-96-485.

Rundberg, R.S., I. Partom, M.A. Ott, A.J. Mitchell and K. Birdsell, (1987). “Diffusion of Nonsorbing Tracers in Yucca Mountain Tuff,” YMP Milestone R524, Los Alamos National Laboratory.

Shreve J.K. and D.M.C. Thomas, (1965). “Operation Roller Coaster -A Joint Field Operation of the Department of Defense, the Atomic Energy Commission, and the United Kingdom Atomic Energy Authority, Defense Atomic Support Agency (unclassified) document DASA-1644.

Stimac, J.A. and D.E. Broxton, (unpublished). “Preliminary Stratigraphy of Tuffs from Borehole 49-2-700-1 at Technical Area 49, Los Alamos National Laboratory, New Mexico,” Los Alamos National Laboratory document.

Stumm W. and J.J. Morgan, (1981). “Aquatic chemistry: an introduction emphasizing chemical equilibria in natural waters,” [2d ed.], New York: Wiley.

Travis, B.J. and H.E. Nuttall (1987). Two-Dimensional Numerical Simulation of Geochemical Transport in Yucca Mountain,” Los Alamos National Laboratory manuscript LA-10532-MS.

van Genuchten, M.T., (1980). “A Closed-Form Equation for Predicting the Hydraulic Conductivity of Unsaturated Soils,” Soil Science Society of America Journal 44, 892-898

Vaniman, D., G. Cole, J. Gardner, J. Conaway, D. Broxton, S. Reneau, M. Rice, G. WoldeGabriel, J. Blossom, and F. Goff, (1996). “Development of a Site-Wide Geologic Model for Los Alamos National Laboratory,” Los Alamos National Laboratory unpublished document.

Wilson, C.R. and K. Kisiel, (1998, unpublished). “Estimated Water Volumes Available to Material Disposal Area AB, Area 2, at Los Alamos National Laboratory”.

Wolfsberg, K., (1980). “Sorptive Properties of Tuff and Nuclide Transport and Retardation” in “Evaluation of Tuff as a Medium for Nuclear Waste Repository: Interim Status Report on the Properties of Tuff,” J.K. Johnstone and K. Wolfsberg, Eds., Sandia National Laboratory report SAND80-1464.

Zyvoloski, G.A., B.A. Robinson, Z.V. Dash, and L.L. Trease, (1997). “Summary of the Models and Methods for the FEHM Application - A Finite Element Heat- and Mass-Transfer Code,” Los Alamos National Laboratory manuscript LA-13307-MS.